CERN-LCGAPP-2007-02
March 22, 2007
Version 1.1

Hadronic Shower Shape Studies in Geant4

J. Apostolakis, G. Folger, V. Grichine, A. Howard, V. Ivanchenko, M. Kossov, A. Ribon
CERN PH-SFT

Abstract

This note describes the studies, undertaken since early 2006, dedicated to understand and improve the simulation of hadronic shower shapes in GEANT4 for high-energy calorimetry applications. In particular, use cases relevant for LHC experiments have been studied. This report provides an overview of the various avenues of investigation taken so far, and presents key results and the current status of these studies. It summarises our assessment, provides an outlook for further studies and directions of research.

1 Motivation

A reasonable simulation of the hadronic shower development of high-energy particles impinging on calorimeters is an essential ingredient to obtain reliable Monte Carlo samples to be used for designing future experiments, calibrating and undestanding detectors, and for physics analyses. Given the rising role that calorimeters are playing as the beam energy increases, coupled with the growing dimensions and complexity of the detectors, the simulation of hadronic showers will be even more important for LHC and ILC experiments.

We recommend the interested reader to consult [1] for a detailed discussion of calorimetry in high-energy physics, together with subjects such as electromagnetic and hadronic showers, providing an ample and updated source of bibliography.

Several test-beam set-ups, carried out at CERN in the last ten years in preparation for the LHC experiments, have tested detector simulations under different conditions, in terms of materials, thicknesses, beam particles, and beam energies [2]. We concentrate here on the validations of the GEANT4 simulation toolkit [3]. For electromagnetic showers, *i.e.* showers started by electrons, positrons and gammas, the test-beam results show that GEANT4 simulations reproduce quite well the data. For hadronic showers. *i.e.* showers started by hadrons (mostly pions, kaons, protons and neutrons), GEANT4 simulations are in good agreement with test-beam data as far as energy response, energy resolution, and e/π are concerned, especially when theoretical based models are used instead of parameterizations [4]. But for shower shapes, *i.e.* for the longitudinal and lateral development of the showers, it is the

other way around: the more sophisticated models of GEANT4 produce showers that are clearly more compact *i.e.* starting earliear, shorter and narrower than the data, whereas GEANT4 parametrized models seem to agree better with the data [4].

These results unambiguously imply that the hadronic shower shapes description in GEANT4 must be improved. Because the development of hadronic showers is the complex result of many different physics processes, we think that, before making any change to the code, it is essential first to have an understanding of how each physics process and model affect the shower, and assess each of these components with thin target data.

The aim of this report is to illustrate the main activities that have been carried out so far to tackle the difficult problem of the shower shapes in GEANT4 .

The structure of the note is the following: we first describe the strategy we follow; then we explain our set-up and the observables we consider; afterwards we offer an overview of GEANT4 hadronic models; we then compare different Physics Lists; thin target benchmarks are presented to validate specific GEANT4 models; then we treat some of the hadronic physics aspects that are important for hadronic showers, as hadronic cross-sections, hadronic elastic scattering, and diffraction; followed by a description of some recent developments on the effects of pions and kaons below 10 GeV, tests of new models (INCL+ABLA, Fritiof, QGSC_EFLOW); finally, we conclude with a summary and future activities.

2 Strategy

Both the cross-sections and the modelling of several physics processes can have an influence in the hadronic shower development. It would be wrong to use calorimeter (thick-target) test-beam data to tune or improve some of these processes, because the observables are the convolution of many effects, impossible to disentagle and would fail in independent applications. Our approach is instead based on thin-target data to validate and eventually tune or improve each process separately and independently. However, we do use calorimeter set-ups to assess the sensitivity of hadronic shower shapes for individual processes, in order to focus on the most relevant for our goal of improving the simulation of shower profiles.

Although any possible improvement in GEANT4 physics models, driven by thin-target data, will be eventually validated by the experiments using their calorimeter test-beam data, it is very convenient to simulate simplified calorimeter set-ups to study the impact of these changes on hadronic showers. There are essentially three advantages of using simplified calorimeters instead of full, real test-beam set-ups. First, we can get quick results, without the need to ask frequently to the experiments to repeat their CPU-consuming productions of simulated samples and complex data analyses. Second, we can concentrate only on pure physics effects related to the shower, without corcern for instrumental effects (like beam composition, beam spread, recombination/quench effects, noise, cross-talk, clustering and reconstruction), which

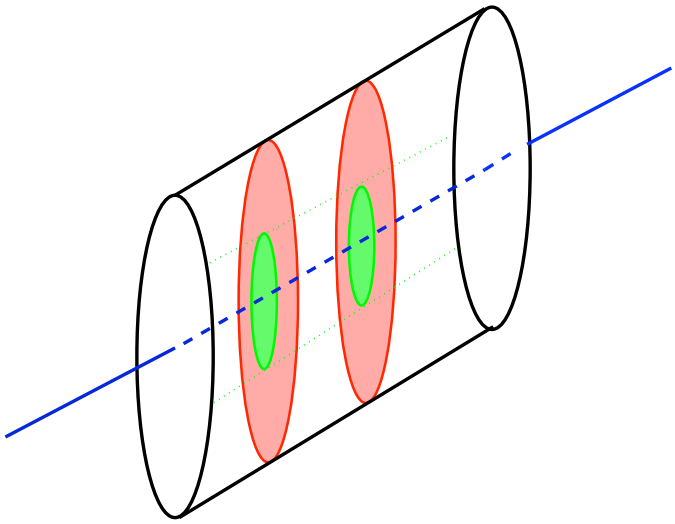

Figure 1: Sketch of the calorimeter set-up.

are instead essential for a meaningful comparison against data. Third, without the "limitation" of looking only to experimentally accessible observables, we can study more variables that could help in our understanding of the development of hadronic showers.

3 Simplified calorimeters and observables

We use a GEANT4 application which consists of a simple cylindrical sampling calorimeter. The materials for the absorber and active components, the number and thickness of the active layers, the radius of the calorimeter, the total length of the calorimeter, and an artificial division of the active layers in radial rings (for studying the radial profile) can all be dynamically specified at run-time. The aim is to reproduce, in a simplified way all the calorimeters of the LHC experiments. In Fig.1 you can see a sketch of the set-up.

The results presented in this note are based on a Copper-Liquid Argon (hereafter Cu-LAr) calorimeter, a kind of simplified "ATLAS HEC", with 60 layers, each made of 25 mm Cu (absorber) and 8.5 mm LAr (active material), corresponding to a length of about 10 λ (nuclear interaction lengths in copper). The diameter of the calorimeter is 150 cm. For studying the longitudinal shower profile, we consider 20 "readout layers", *i.e.* equally spaced samplings in which we sum together the energy deposits from each set of three consecutive active layers. For the lateral shower profile, we define 10 radial rings, with size increasing linearly with the radius (0.1 λ the first, 0.2 λ the second, etc., with the last one defined to include any contribution at larger radius but inside the calorimeter); the energy deposit in one ring is defined as the sum of the energy deposits in all layers contained within the corresponding ranges of

distances from the calorimeter's axis (the beam particles are always shot along the axis of the cylindrical calorimeter).

We consider π^- and e^- beam particles with kinetic energies: 30, 100, and 300 GeV. The observables that we consider are the following:

- E_{vis} : the average visible energy, *i.e.* the sum of the energies deposited in each active layer;
- E_{tot} : the average total energy deposited in the whole calorimeter;
- σ_E/E : energy resolution; the notation is a shorthand for precisely: $\sigma_{E_{vis}}/E_{vis}$;
- e/π : ratio between the average visible energy for an electron beam, and the average visible energy for a pion beam of the same energy;
- $E_{vis}^{(layer\ i)}$: the energy deposited in each "readout layer", with $i = 1, ..., 20$ (from which we get the longitudinal shower profile);
- $E_{vis}^{(ring\ j)}$: the energy deposited in each radial ring, with $j = 1, ..., 10$ (summed over all active layers, from which we get the lateral shower profile);
- *exit_kin* : the exiting kinetic energy per event, *i.e.* the average sum of the kinetic energies of all tracks exiting the calorimeter in an event;
  we consider also the fraction of the exiting kinetic energy which is due to some particle types, *e.g.* neutrons, gammas, neutrinos, muons, etc, and the average number of these tracks per event; we will use later the following two variables:
  - *exit_fn* : fraction of the exiting kinetic energy due to neutrons;
  - *exit_#n* : average number of exiting neutrons per event;
- the average number of created tracks (and steps as well) per event, for different particle types; in particular, we will use the following variables:
  - $\#EM$: average number of electron, positron, and gamma tracks per event;
  - $\#\pi$: average number of pion (neutral and charged) tracks per event;
  - π^0/π : ratio between the average number of neutral pion tracks and the average number of pion (neutral and charged) tracks;
  - $\#p$: average number of proton tracks per event;
  - $\#n$: average number of neutron tracks per event;
- the average track length inside the calorimeter, for different particle types; we will use the following variable:
  - L_n : average track length for neutrons (fully inside the calorimeter);

- kinetic energy spectra of different particle types (electrons/positrons; gammas; charged pions; charged kaons; protons; neutrons) at each active layer;

- the visible energy contribution, total, layer by layer, ring by ring, of different particle types (electrons/positrons; muons; charged pions; charged kaons; protons/antiprotons; neutrons/ions : notice that we group together neutrons and ions because, since GEANT4 version 8.1, neutrons can deposit energy, which corresponds physically to elastic recoiled nuclei with kinetic energies below a certain threshold, currently fixed at 100 keV, without producing the secondary).

Notice that most of the above "observables" are not experimentally measurable in practice, but still worth study, as they provide rich information useful for understanding the development of hadronic showers.

In order to summarize the information on shower shapes we will use often the following variables:

- f_{L1} : fraction of the visible energy in the first quarter of the calorimeter, *i.e.* in the first 15 active layers (or 5 "readout layers", corresponding to the first 2.5 λ of the calorimeter);

- f_{L2} : fraction of the visible energy in the second quarter of the calorimeter (corresponding to the second 2.5 λ of the calorimeter);

- f_{L3} : fraction of the visible energy in the third quarter of the calorimeter (corresponding to the third 2.5 λ of the calorimeter);

- f_{L4} : fraction of the visible energy in the last quarter of the calorimeter (corresponding to the last 2.5 λ of the calorimeter);

- f_{R1} : fraction of the visible energy in the first three radial rings;

- f_{R2} : fraction of the visible energy in the second three radial rings;

- f_{R3} : fraction of the visible energy in the remaining radial rings.

By definition, $f_{L1} + f_{L2} + f_{L3} + f_{L4} = 1$, and $f_{R1} + f_{R2} + f_{R3} = 1$.
To give an example of the physical meaning of these variables, compact hadronic showers have larger f_{L1}, f_{L2}, f_{R1}, and smaller f_{L3}, f_{L4}, f_{R2}, f_{R3}. This is the case for hadronic showers generated with GEANT4 QGSP Physics List with respect to the ones observed experimentally in calorimeter test-beam data.
As already said before, we monitor the contribution of the visible energy, also layer by layer and ring by ring, due to specific types of particles, therefore it is possible to define also for these the variables describing, respectively, the fraction of the visible energy due to this particle type, the longitudinal and lateral fractions (the sum of which is still normalized to 1):

- e_E_{vis}, e_f_{L1}, e_f_{L2}, e_f_{L3}, e_f_{L4}, e_f_{R1}, e_f_{R2}, e_f_{R3} : for electrons and positrons;
- p_E_{vis}, p_f_{L1}, p_f_{L2}, p_f_{L3}, p_f_{L4}, p_f_{R1}, p_f_{R2}, p_f_{R3} : for protons and antiprotons;
- π_E_{vis}, π_f_{L1}, π_f_{L2}, π_f_{L3}, π_f_{L4}, π_f_{R1}, π_f_{R2}, π_f_{R3} : for charged pions;
- n_E_{vis}, n_f_{L1}, n_f_{L2}, n_f_{L3}, n_f_{L4}, n_f_{R1}, n_f_{R2}, n_f_{R3} : for neutrons, antineutrons, and nuclei;
- k_E_{vis}, k_f_{L1}, k_f_{L2}, k_f_{L3}, k_f_{L4}, k_f_{R1}, k_f_{R2}, k_f_{R3} : for charged kaons;
- μ_E_{vis}, μ_f_{L1}, μ_f_{L2}, μ_f_{L3}, μ_f_{L4}, μ_f_{R1}, μ_f_{R2}, μ_f_{R3} : for muons.

4 Overview of GEANT4 hadronic models

GEANT4 includes cross-sections and physics models for hadronic interactions from thermal energies (for neutrons) to hundreds of GeV. For many regimes, a choice of physics model is available, enabling a user to choose between more precision and better CPU performance.

At high energies ($E \gtrsim 20$ GeV) the Quark-Gluon String (QGS) model and a Fritiof-like String model (FTF) provide theory-driven interaction models of the initial projectile-nucleon collision.

At energies below $E \sim 10$ GeV, two cascade models are provided, one following the Bertini approach, and one, called the Binary cascade, which is more theory-based. Each of these models simulates the initial interaction within the nucleus, producing high energy secondaries and leaving the nucleus in a highly excited state. A number of models are available to perform the de-excitation. One is the GEANT4 precompound model [6] that starts by decaying the excitons formed during the high energy interactions or cascades. It then calls one or more of the available fission, Fermi breakup, multi-fragmentation and evaporation routines. The precompound model is currently used as a "back-end" for the QGS and Binary cascade models.

The Bertini-type cascade employs its own evaporation model to de-excite the remnant nucleus.

The slowest remaining particles may also be re-absorbed by the nucleus. They may be treated by the Chiral Invariant Phase space (CHIPS) model, which may also be used as a back-end for the QGS model.

For low energy projectiles ($E < 20$ MeV), high-precision neutron processes and photo-evaporation codes are provided, each of which rely on data libraries that are provided with GEANT4 .

For photo-nuclear and electro-nuclear interactions processes are provided that use the CHIPS model. Stopping particles are treated utilising a CHIPS-based capture process.

Covering all long-lived particles at all energies are the Low Energy Parametrized (LEP) and High Energy Parametrized (HEP) models that have their origins in the GHEISHA hadronic package [7] as used with Geant3. The GHEISHA Fortran code was cast into C++, re-engineered and split into the current high- and low-energy parts, and a number of corrections and improvements were undertaken. These processes utilise simplified descriptions of interaction mechanisms, with key quantities parametrized for speed. They cover all long-lived hadrons, and were designed to describe hadronic showers reasonably well. They are also intended to conserve energy and momentum on average but not event by event.

The LEP models are especially important because they cover the transition region between the cascade models and the string models (between 10 and 20 GeV), which for some particles is not covered by the theory-driven models.

The LEP and HEP models provide faster alternatives to the theory-driven models mentioned earlier. In addition they are utilised for long-lived hadrons (Ω, Σ), due to a lack of alternatives, and to cover the transition between the cascade and string model regions of applicability.

The universal elastic model is derived from GHEISHA and has been used in most Physics Lists. Specific models exist for coherent p-p and p-n elastic scattering[8]. New Glauber-based elastic scattering model have been recently delivered. A new process, QElastic, including cross-sections and final state models, has been developed for proton and neutron scattering on nuclei.

In the following discussion, four of the most-used models (QGS, Bertini-type and Binary cascades, CHIPS) will be overviewed.

Models at high energies

The QGS model [9] is used in GEANT4 to simulate the interactions of protons, neutrons, pions and kaons with nuclei, in the approximate energy range 12 GeV to 50 TeV. Other models are coupled to it to fragment and de-excite the damaged nucleus after the initial high energy interaction.

The model selects a target nucleon from a detailed, three-dimensional model of the nucleus, splits the projectile and target nucleon into quarks and di-quarks, and then forms and excites quark-gluon strings. Strings are stretched between partons of the projectile and target nucleon, using sampled parton densities. Hadronization proceeds by longitudinal string fragmentation in which the string is successively broken into a hadron and another string until the string mass becomes low enough to break into two hadrons.

The transverse momentum distribution is sampled from a Gaussian distribution, while the longitudinal momentum distribution is sampled from fragmentation functions. The amount of diffractive dissociation is chosen empirically.

This is the principal model for incident particles above 12 GeV in the QGSP Physics Lists, used by LHC experiments (ATLAS, CMS, LHCb) for their main production simulations.

Bertini-type cascade

In the cascade energy range GEANT4 has a Bertini-type cascade model which handles incident nucleons, pions, kaons and hyperons up to 10 GeV. It follows the INUCL implementation of N. Stepanov [10] and uses standard intra-nuclear cascade features of the Bertini approach [11].

Step-like nuclear density distributions and potentials are used. Since experimental cross-sections and angular distributions are used, the model can be extended to any hadron for which sufficient experimental data are available.

The projectile (and induced secondaries) is transported along straight lines through the nuclear medium and interacts using the free hadron-nucleon total cross-section. The nuclear medium is approximated by (up to three) concentric, constant-density shells. At shell boundaries a particle can be reflected or transmitted.

As cascade collisions occur, an excited residual nucleus is built up. An exciton decay routine is then used to de-excite the nucleus. For light, highly-excited nuclei Fermi breakup may occur, and a fission channel is available. A custom nuclear evaporation routine for neutrons and alphas is followed by gamma emission at the lowest excitation energies (< 0.1 MeV).

Binary cascade

The GEANT4 Binary cascade model [12] is valid for incident protons and neutrons with $E_{kin} < 3$ GeV, pions with $E_{kin} < 1.5$ GeV, and light ions with $E_{kin} < 3$ GeV/A, but it can be used in some cases adequately up to 10 GeV.

The model is based on two-body to two-body, or two-body to one-body interactions within the target nucleus. Nucleon-nucleon scattering is done by resonance formation and decay. Elastic nucleon-nucleon scattering is also included. Meson-nucleon inelastic scattering, except for true absorption, is modelled as s-channel resonance excitation. Once resonances are formed they may interact with other nucleons or decay.

Target nucleons are sampled from a detailed three-dimensional nuclear model and the particle-particle collisions within it are approximated by free cross-sections. The incident particle and subsequent secondaries propagate through the nucleus along curved paths, which are calculated by numerical integration from the equation of motion.

When the cascade phase is finished, the GEANT4 precompound model is used to de-excite the residual nucleus.

Chiral Invariant Phase Space Model

The Chiral Invariant Phase Space (CHIPS) model has its origins as an event generator [13, 14] first incorporated into GEANT4 for treating anti-baryon-nucleon annihilation, the capture of negatively charged hadrons at rest, and gamma- and lepto-nuclear reactions. It is also used in some GEANT4 Physics Lists to handle the

nuclear fragmentation part of nuclear de-excitation.

The basic building block of this model is the quasmon - a collection of massless free partons, which form hadronic systems. A critical temperature T_c relates the quasmon mass M_Q to the number of its partons n. Hadronization proceeds via quark fusion and quark exchange.

In the model, u, d, and s quarks are treated as massless and related by chiral symmetry. It can produce kaons, using a strangeness suppression parameter to adjust their multiplicity.

Quark exchange or fusion can be considered as a one-dimensional process, since the maximum energy from the primary quark parton contributes to the inclusive spectra. It has been demonstrated experimentally by the fact that when the inclusive hadron spectra are plotted versus $k = (p + E_{kin})/2$, they not only have the same exponential slope but nearly coincide.

5 Comparisons between Physics Lists

GEANT4 provides several Physics Lists, these comprise consistent sets of physics models that cover all materials, beam particle types, and beam energies. They are meant to provide different levels of physics accuracy, and therefore of CPU performance, for different application domains.

A detail comparison of hadronic showers between different Physics Lists, for the same calorimeter configuration and projectile, can provide useful information on the impact of different sets of models on the development of hadronic showers. For instance, by comparing two Physics Lists that have the same cascade and de-excitation part, but differ for the high-energy part, we can evaluate how much the differences between the two high-energy models affect the showers. Similarly, by comparing two Physics Lists that have the same high-energy part, but different cascade and de-excitation models, it is possible to have an idea of the impact of the latter on shower shapes. Another two cases are worth mentioning: comparing Physics Lists that contain either the Bertini-type or Binary cascade models allows us to evaluate the effect of better simulation of intermediate energy hadrons on shower shapes; finally, by comparing two Physics Lists which differ only in the addition of the high-precision treatment of low-energy neutrons (with kinetic energy below 20 MeV), it is possible to have an idea of the effect of such special modelling on the development of showers.

We used GEANT4 version 8.2, with default production range cut (0.7 mm), and each run consisted of 5000 events. In the tables 1, 2, and 3 the comparisons are made between various observables (defined in section 3) for different Physics Lists, for π^- beams of 30, 100, 300 GeV, respectively. In the first column we specify the unity, if any, and give the typical statistical error.

Notice that the average number of tracks per event, for different particle types, have been obtained with the environmental variable AlwaysKillLeadingHadron defined. This means that for any hadronic inelastic interaction the incoming track is always

killed, and if a particle of the same type appears in the final state it is associated to a new track. If instead the default is used (*i.e.* AlwaysKillLeadingHadron undefined), then the counting of some particles, in particular for charged pions, would be reduced, and this would imply an artificially high π^0/π fraction, which could be wrongly interpreted.

Some observations on the results:

- As far as the visible energy is concerned, LHEP has the lowest visible energy, the worst resolution (*i.e.* the highest σ_E/E), and the highest e/π; conversely, Physics Lists with an intra-nuclear cascade model (Bertini-type or Binary) have the largest visible energy, the best resolution, and the lowest e/π.

- As far as the shower profiles are concerned, QGSP, QGSP_EMV, and QGSC are quite similar, which brings two conclusions. First, the major revision of the electromagnetic multiple scattering between GEANT4 version 7 (used in QGSP_EMV) and 8 (used in QGSP) does not have any significant impact on hadronic shower shapes. Second, replacing the Precompound model (used in QGSP) with the Chiral Invariant Phase Space model (used in QGSC) seems also not relevant for hadronic showers at high energies. It is however important to notice that both QGSP and QGSC use the same parametrized model for particles below roughly 10 GeV, so it would be wrong to conclude that hadronic models for the low-energy part (de-excitation and evaporation) are not important for hadronic showers. We will come back to this point in section 11.
  A variant of the QGSC Physics List, QGSC_EFLOW, which will be discussed in section 12, does produce wider showers, however.

- The effect of intra-nuclear cascade models, Binary (used in QGSP_BIC) and Bertini-type (used in QGSP_BERT), is to make the showers longer and wider, hence in the right direction with respect the test-beam data (whereas the changes in energy resolution and e/π need to be checked, because LHEP and QGSP were describing the data reasonably well). This trend is stronger in the case of QGSP_BERT than in QGSP_BIC, the main reason being the different range in which the cascade models are applied for pions and kaons (indeed, the latter are not treated by Binary cascade): below about 10 GeV, in the case of Bertini-type cascade, and below 1.3 GeV in the case of Binary model.

- Using the precise transportation of low energy neutrons (*i.e.* with kinetic energies below about 20 MeV), which is activated in the _HP extensions of Physics Lists, the hadronic showers are a bit longer and wider, but the effect is small and mostly on the tails of the longitudinal and lateral shapes.

- As far as the contribution of different particle types on hadronic showers is concerned, we can make the following observations:

- for the visible energy, electrons give the largest contribution, which increases with the beam energy, followed by protons, then charged pions, and finally ions (kaons and muons give negligible values);
- for the shower shape, the electron contribution is the shortest and narrowest, whereas the other contributions are similar, with the protons being the longest and widest;
- LHEP has a significantly smaller electromagnetic fraction (*i.e.* fraction of the visible energy due to electrons and positrons) than all the other Physics Lists.

From these facts, and given that the LHC calorimeter test-beams show that LHEP describes the longitudinal profile of hadronic showers well at high energies, a reasonable explanation for the fact that QGSP produces shorter and narrower showers could be that it has a too high electromagnetic fraction, likely due to an overproduction of π^0. We will come back to this point, from another direction, in section 11.

6 Validating high-energy models with thin target data

The validation of models used to simulate hadronic interactions is based on comparisons with thin target experiments. In these experiments the target thickness is chosen such that the fractions of particles undergoing inelastic interactions is sufficient to perform the experiment, but low enough that secondary interactions are not important and can be corrected for. Therefore, the experimental results are a direct measure of the properties of a single inelastic reaction.

In general, these experiments provide differential cross-sections or rates as a function of one or two variables. The variables include rapidity, transverse energy or momentum, or Feynman x measuring the longitudinal momentum fraction.

For a good validation of models, data for particles relevant in hadronic showers (charged pions, proton, neutron, kaons) used as beam particles, and impinging on targets covering a range from light to heavy nuclei would be needed. Experimental data, however, are not as rich: there are more data with proton beams than with pion beams, and often the measurement of secondaries is limited. Models like QGS do have separate parameter sets for different primary particles types. For example, the parameter describing the number of nucleons that the primary interacts with, in a given nucleus, is different for protons and pions. There is a need to validate a given model for all particles relevant in hadronic showers.

We base the current validation of GEANT4 hadronic physics on the following publications:

- Backward production of pions and kaons in the interaction of 400 GeV/c protons with nuclei [17];

- Inclusive charged pion production in hadron-nucleus interactions at 100 GeV/c and 320 GeV/c [15];

- Rapidity and transverse momentum structure in π^+ and $^+$ collisions with Al and Au nuclei at 250 GeV/c [18];

- Inclusive production of charged pions in p-C collisions at 158 GeV/c beam momentum [21];

- Inclusive production of π^0 mesons in $\pi - p$, $k - p$ and $\gamma - p$ collisions at energies around 100 GeV [19];

- Production of hadrons with large $P^{\perp}$ in nuclei at 70 GeV [20];

- Measurement of particle production in proton induced reactions at 14.6 GeV/c [22].

Simulation of these experiments can be done in two ways. First, one can simulate the complete experiment, and apply the same cuts and corrections to the simulated data as for the experimental data. Second, one can only simulate the reaction of the beam particle with a nucleus of the target ignoring the simulation of the experimental set-up. The first method will give more precise results, as experimental effects are better accounted for; however, the simulation time will be long, as most beam particles pass the thin target without any interaction. The second method is simpler and allows to get good statistical precision; if experimental effects are well corrected for in the published data, this will give results very similar to the first method. We use this second method for the validation of the high energy models.

The Physics List that reproduces rather well the longitudinal shower profile, LHEP, uses the same models for low energies as the QGSP Physics List. Therefore, we started to compare the QGS model with thin target experimental data at high energies.

An experiment carried out at Fermilab by J. J. Whitmore *et al.* [15] studied pion production from some nuclei (magnesium, silver and gold) for incident $\pi^{\pm}$, K^+, p and $\overline{p}$ of 100 GeV/c and for π^- of 320 GeV/c. The experimental data consist of laboratory rapidity (y) and transverse momentum squared (p_t^2) distributions, and are available from the EXFOR [16] database. Unfortunately, the statistics of the experiment are limited: typically a few hundred events were selected for each combination of target and beam particle. As an example, we show in Fig.2 one of the beam-target combinations with the highest experimental statistics, π^-(100 GeV) Ag $\rightarrow \pi^+ X$, comparing data and the QGS model simulation.

In general, QGS describes the experimental distributions for rapidity very well, especially the high rapidity end. Particles with high rapidity are high energy forward particles and a good description of these particles is important for a reasonable description of the longitudinal shower development. The distributions in transverse momentum squared are in general somewhat too narrow, albeit the difference is less pronounced than in the example shown.

The experiment by N. A. Nikiforov *et al.* [17] measured backward production of particles produced in scattering of 400 GeV protons on nuclei (^{6}Li, Be, C, Al, Cu, Ta). Invariant cross-sections as a function of secondary momentum at fixed angles from 70° to 160° were measured for secondary π^+, π^-, K^+, and K^-. Figure 3 shows a comparision of simulation using the QGS model to experimental data.

A good description of particles produced at large angles is crucial for a good description of the lateral shower shape. Studies of hadronic showers in test beams by ATLAS and CMS collaborations indicate that hadronic showers simulated using the QGSP Physics List are too narrow compared to data. This validation does not show any clear problem in QGS for high energy primary protons, in fact the simulation reproduces the thin target experiment well.

The NA49 collaboration, C. Alt *et al.* [21], measured with high statistics the inclusive production of pions in minimum bias p+C interactions using the NA49 detector at the CERN SPS at 158 GeV/c beam momentum. The data cover transverse momentum p_T up to 1.8 GeV/c and Feynman $x_F = 2p_L/\sqrt{s}$ from -0.1 to 0.5. The data are presented in double differential form, allowing detailed comparison to simulation.

In figure 4 we compare the simulation results using QGS model to experimental data. Simulation describes well the major part of the cross-section, but fails to describe the tails of the distributions of the high statistics data. For small Feynman x_F the simulation underestimates the cross-section for high transverse momenta. For large x_F, in the case of secondary positive pions the agreement within statistic uncertainties is reasonable; for secondary negative pions the QGS model overestimates the cross-section up to a factor of 4. The predicted cross-section is very similar for positive and negaitve pions and does not reflect the suppression seen for forward going negative pions. This discrepancy could be due to a bad modeling of the diffractive part of the inelastic cross-section.

For these data, we also compare with the simulation obtained with the FTF model. This model fails even more than QGS to describe experimental data. However, during these investigations some concerns were raised towards the parameters of the G4PomeronCrossSection class. This class is used by both QGS and FTF to choose the nucleons participating in an interaction. The parameters relevant to the interaction probabilities of primary protons and neutrons with nucleons were tuned for QGS. Using default values for the pomeron parameters, we obtain a much better agreement for this modified FTF model and experimental data, see 5. The test of the effect of this modification on the shower shape did not show any significant change, see 12.

The production of neutral pions is another important factor for a correct de-

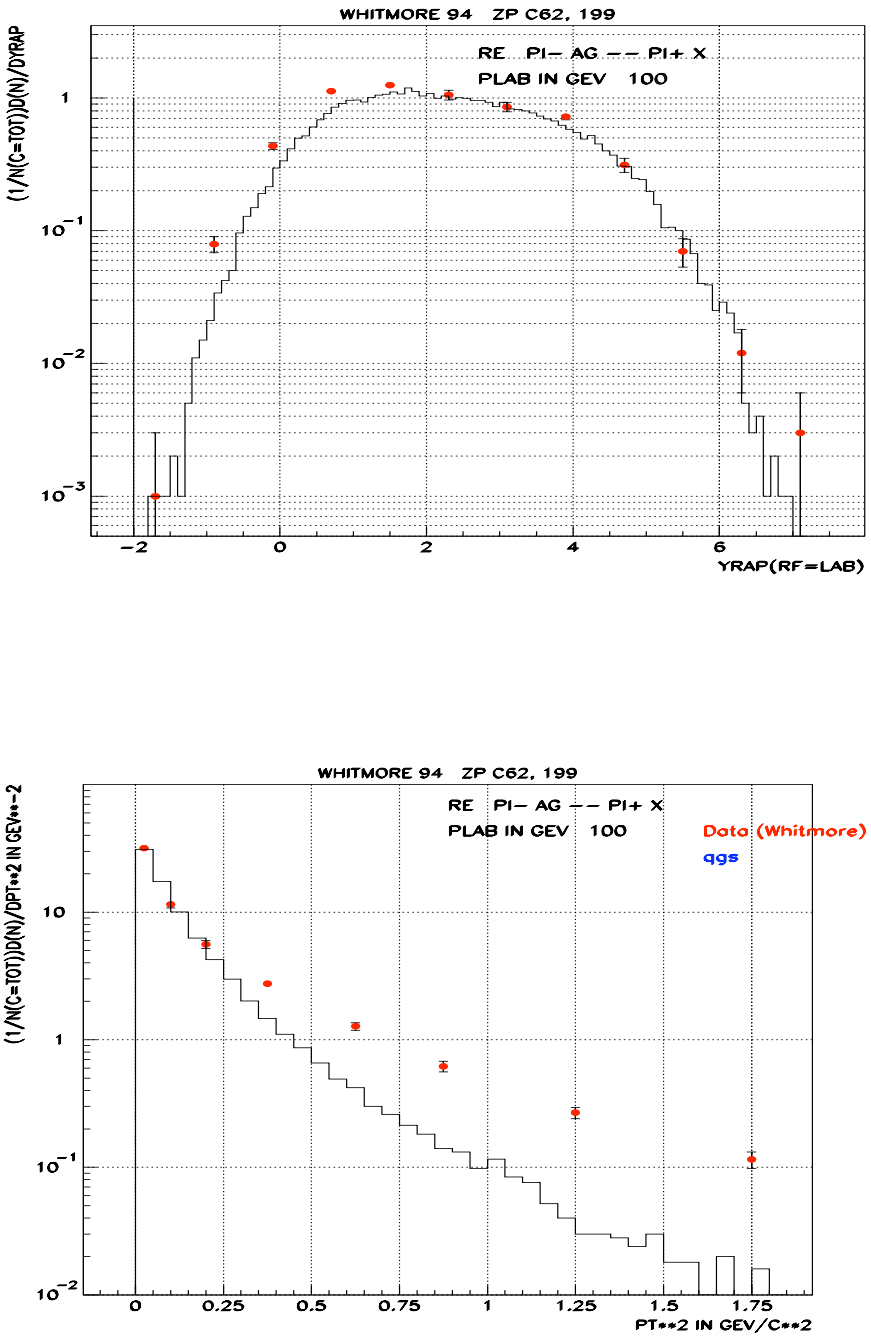

Figure 2: Comparison of QGS simulation (histogram) to experimental data (points) [15]. The upper plot shows rapidity, and the bottom one transverse momentum squared distributions for positive pions produced by negative pions interacting with silver.

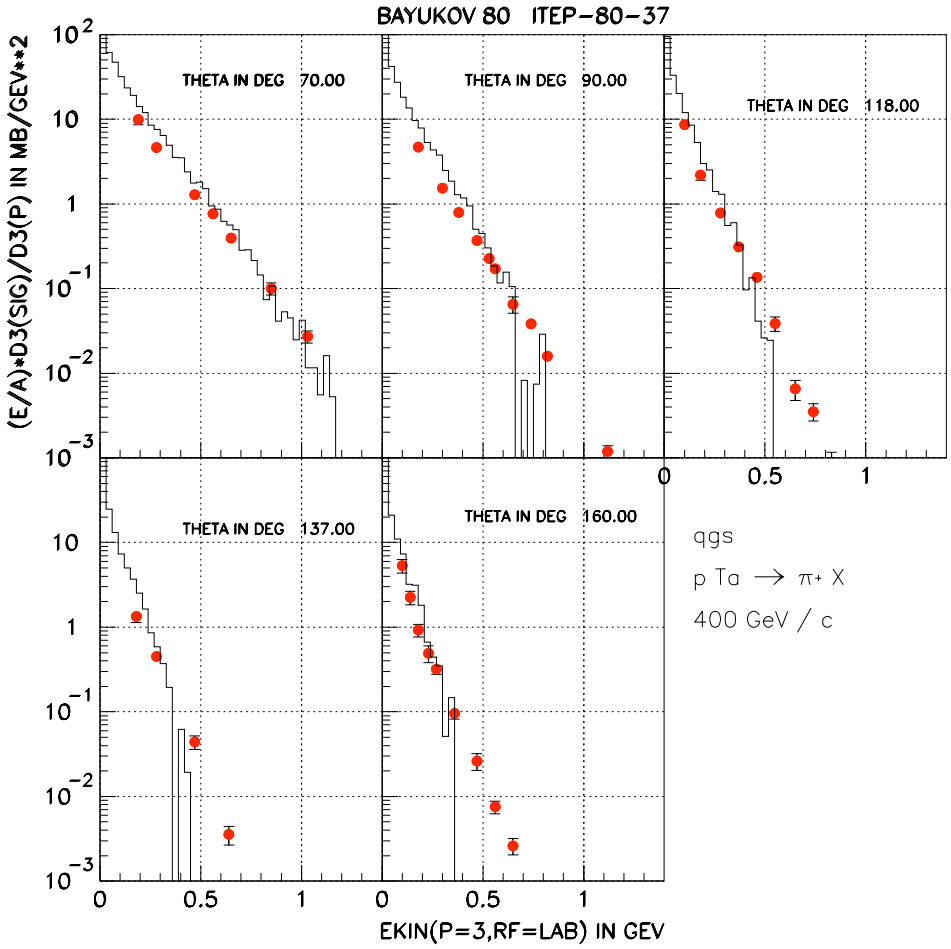

Figure 3: Comparison of QGS model (histogram) to experimental data (points) [17]. Shown here is the invariant cross section for production of positive pions by scattering 400 GeV/c protons on a Tantalum target, as a function of kinetic energy of the secondary pions for five different production angles.

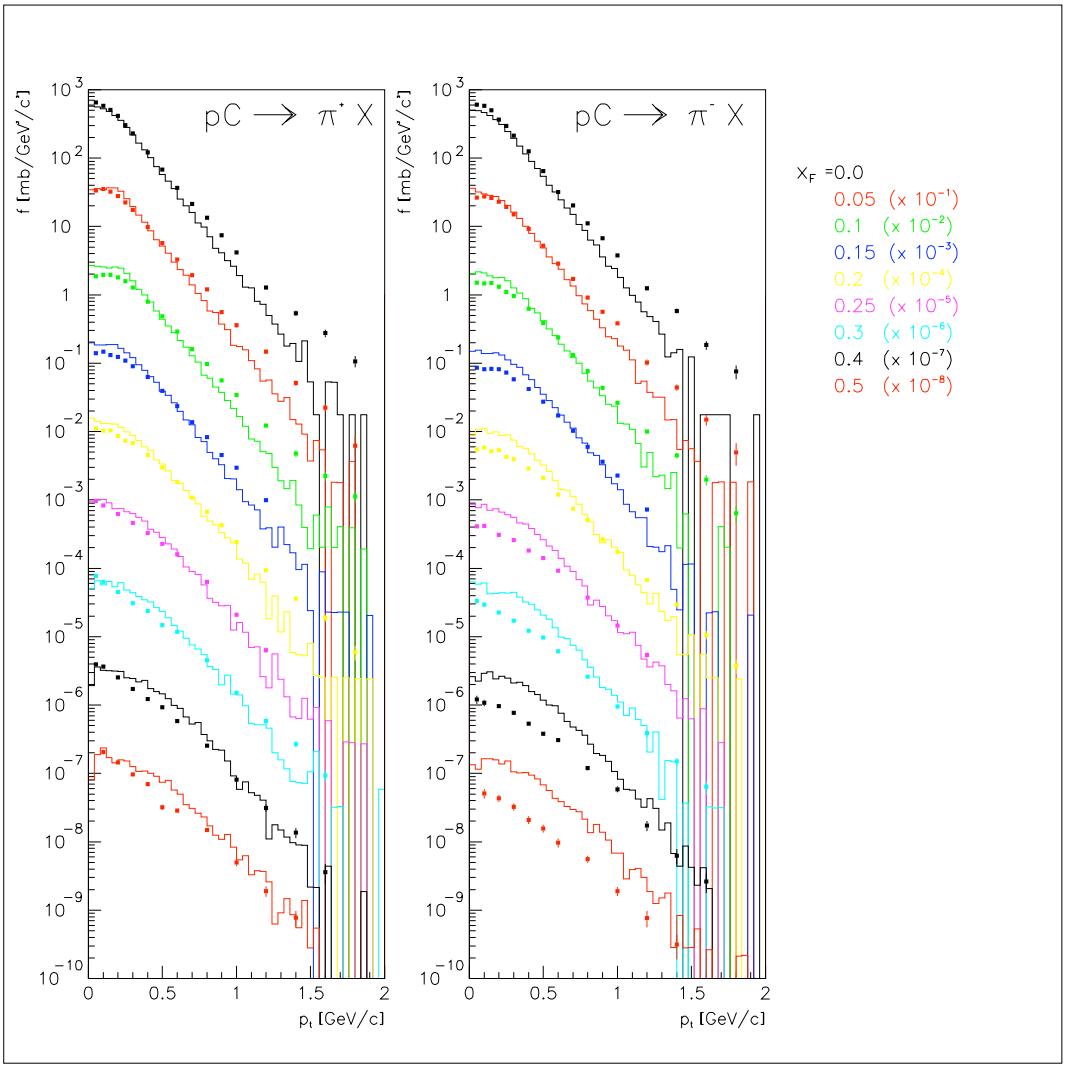

Figure 4: Comparison of QGS model to NA49 data [21]. Points with error bars are experimental data; the histogram shows the QGS model. The left and right plots show the inclusive production cross-section as a function of transverse momentum p_T and Feynman x_F for positive and negative pions in inelastic interactions of protons on Carbon. The curves for increasing x_F are scaled by increasing factors of 10 in order to avoid overlapping curves.

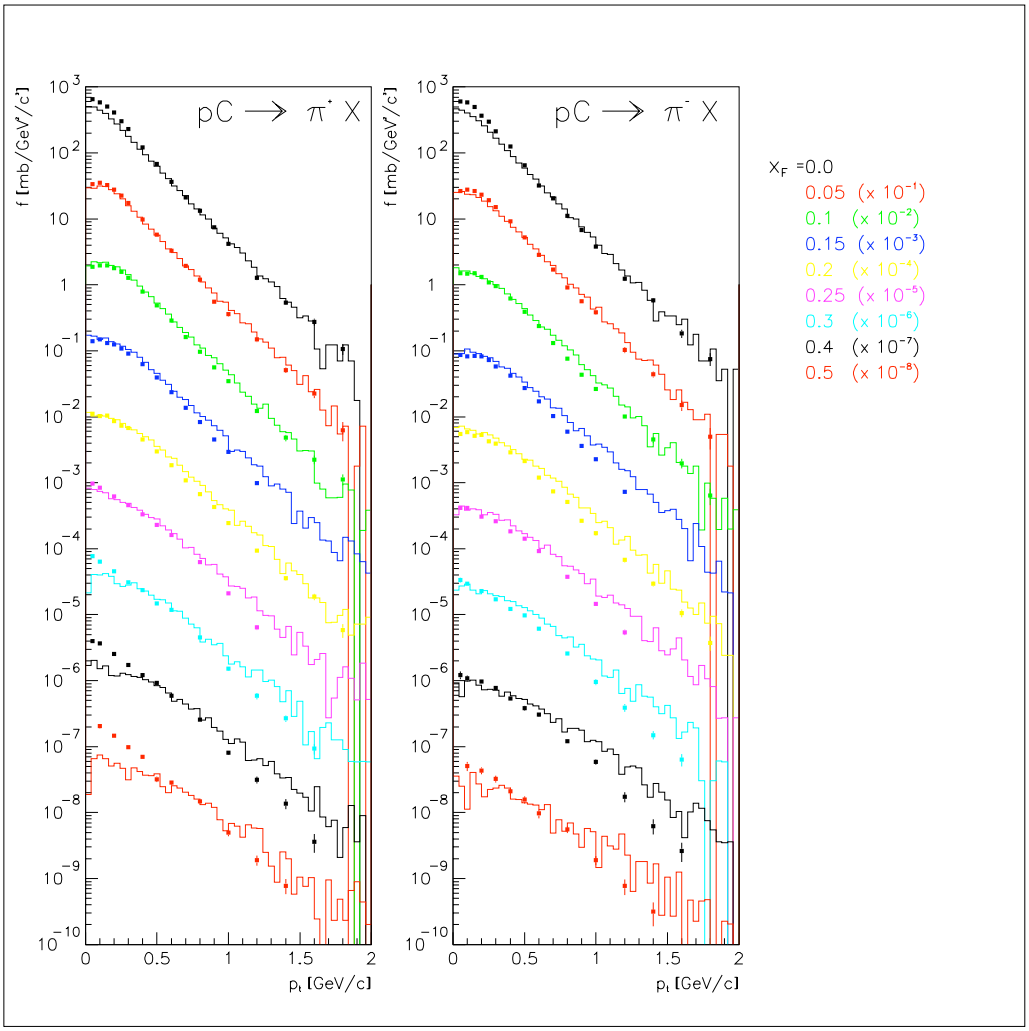

Figure 5: Comparison of a modified FTF model to NA49 data [21]. Points with errors bars are experimental data, the histogram shows the results obtained with the modified FTF model. The left and right plots show the inclusive production cross-section as a function of transverse momentum p_T and Feynman x_F for positive and negative pions in inelastic interactions of protons on Carbon. The curves for increasing x_F are scaled by increasing factors of 10 in order to avoid overlapping curves.

scription of hadronic showers. The short lifetime of neutral pions and their decays exclusively into two photons, or electron and photon, effectively transfer part of the hadronic energy to electromagnetic energy.

We compare the production of neutral pions from interactions of positive and negative pions of 140 GeV/c on hydrogen. The experimental data are from the Omega collaboration, R. J. Apsimon *et.al.* [19]. The experiment measured inclusive production of neutral pions in the beam fragmentation region in collisions of photons, charged pions, and kaons with hydrogen, concentrating on ratios of the production rates for the different beams. The measurements are given as double differential invariant cross-sections as a function of transverse momentum p_t and Feynman x_F, covering a range of p_t up to 2 GeV/c and x_F between 0.1 and 0.8.

In figure 6 we compare the measured invariant cross-section for neutral pion production from π^+H interactions to result obtained from the QGS model. The experiment saw no difference in production cross-section from positive and negative pions, and published only the average; the absolute normalisation of the experimental invariant cross-section is uncertain. For small x_F the QGS model predicts a slightly to steep fall with increasing p_t, while for larger x_F the agreement is good.

7 Hadronic Cross-sections

Hadron-nuclear cross-sections play an important role in the simulation of hadronic calorimeters and particularly for the correct description of the longitudinal shape of hadronic showers. Therefore verification and improvement of total cross-sections and separately elastic and inelastic cross-sections is very important.

GEANT4 has the following models for hadron-nuclear cross-sections:

1. G4HadronCrossSections class for inelastic and elastic hadronic cross-sections, following the GHEISHA approach (which is used in the LHEP Physics List).

2. G4PiNuclearCrossSection (used in the QGSP Physics List) and G4NucleonNuclearCrossSection (under development, results are not included here) classes for Barashenkov parameterization [23]-[24], obtained by the interpolation of total and inelastic cross-sections for pion(π^+,π^-)-nuclear and nucleon(p,n)-nuclear interactions, respectively.

3. G4ProtonInelasticCrossSection class for the Axen-Wellisch parameterization model [25] for proton inelastic cross-sections, used in the QGSP Physics List.

4. G4GlauberGribovCrossSection (new) class for total and inelastic hadron-nuclear cross-sections in the Glauber model with Gribov improvements (GG model).

5. G4QInelasticCrossSection (under development) class of the CHIPS sub-package of GEANT4 for inelastic hadron cross-sections.

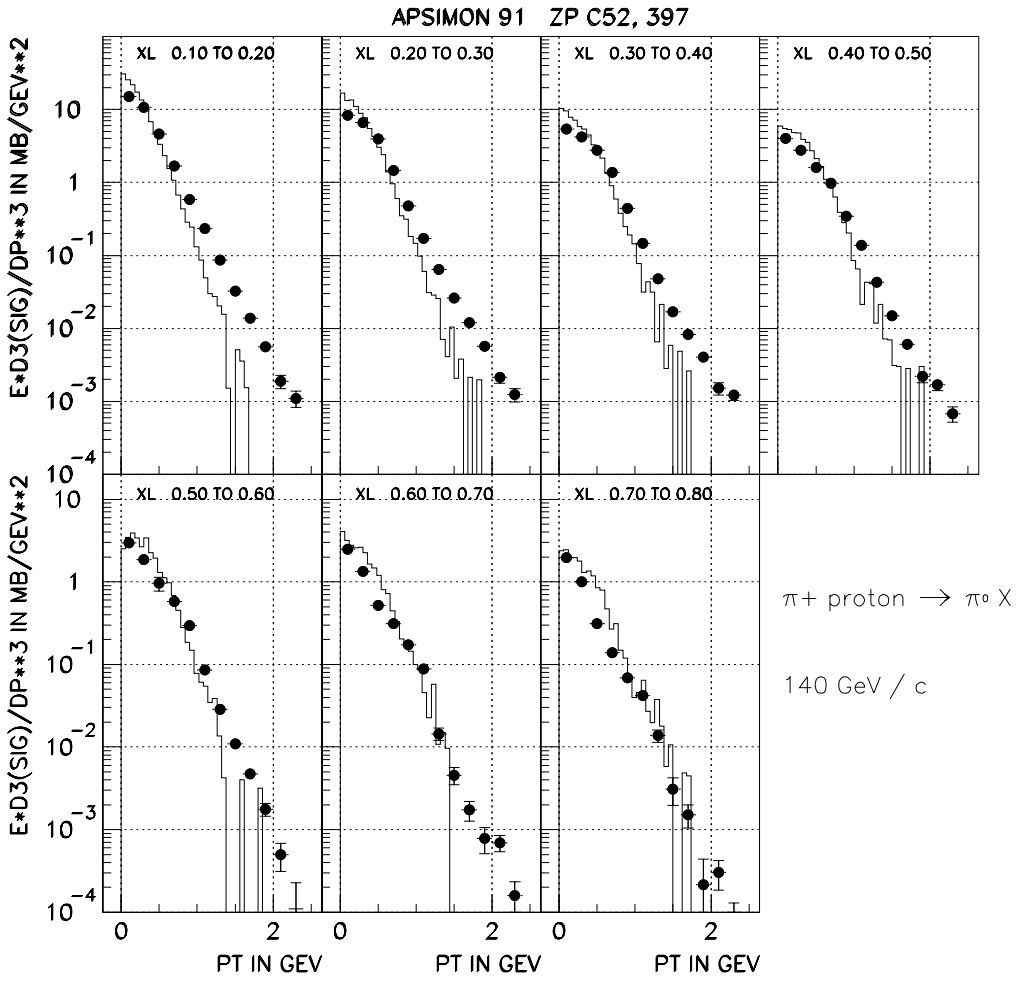

Figure 6: Invariant cross-section of neutral pion production in π^+H interactions as a function of p_T for seven intervals in x_F from 0.1 to 0.8. Points are experimental data from the Omega collaboration [19] with error bars representing statistical errors only; the histogram shows the results obtained with the QGS model.

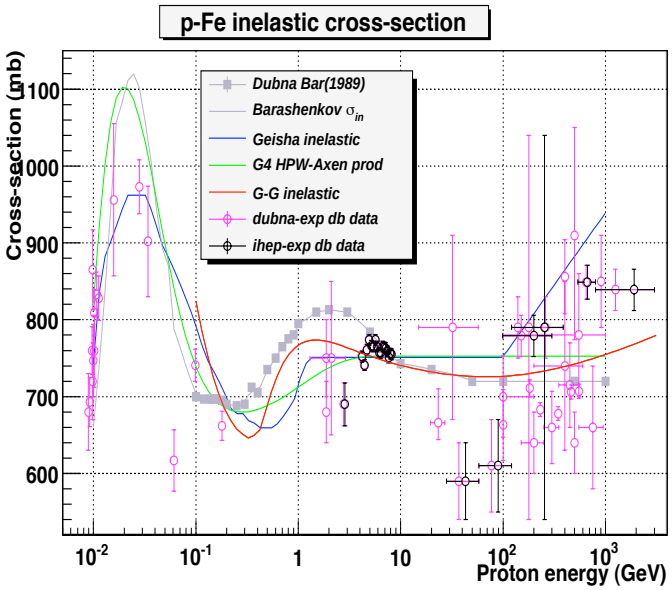

Figure 7: Inelastic cross-sections of protons on an Iron target. Open points are used for experimental data from [27]-[28]; lines correspond to different GEANT4 models; closed points are Barashenkov parameterization [24].

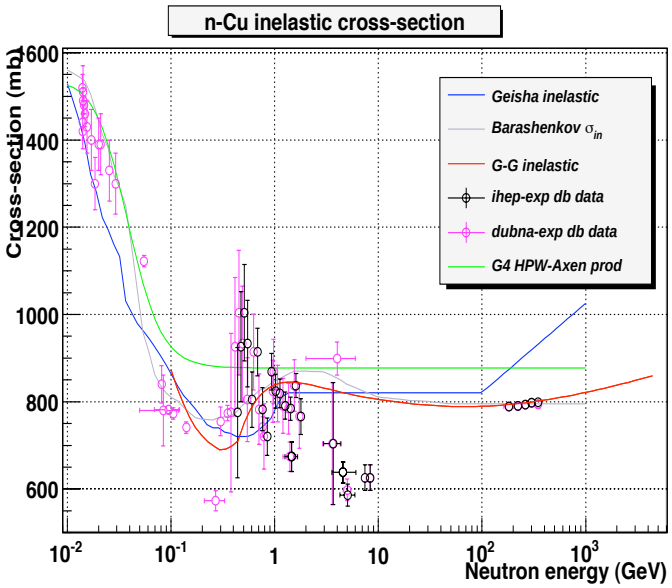

Figure 8: Inelastic cross-sections of protons on a Copper target. Open points are used for experimental data from [27]-[28]; lines correspond to different GEANT4 models.

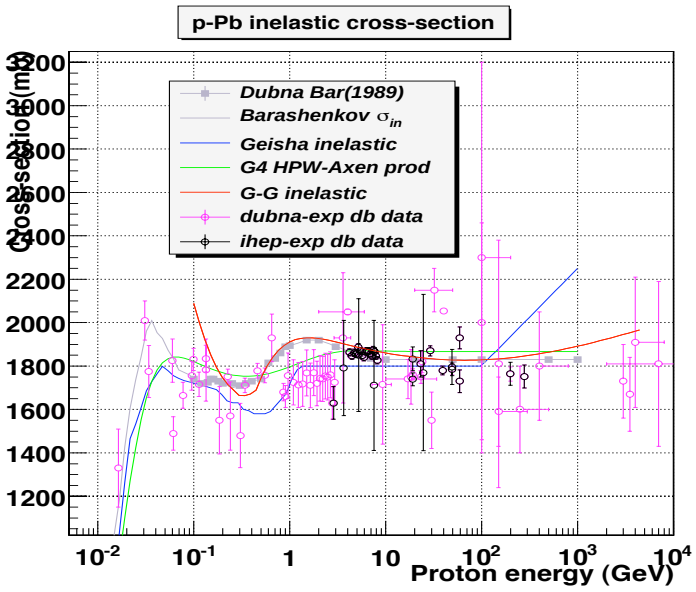

Figure 9: Total cross-sections of protons on a Lead target. Open points are used for experimental data from [27]-[28]; lines correspond to different GEANT4 models; closed points are Barashenkov parameterization [24].

Comparisons have been undertaken for protons, neutrons, π^+ and π^- on C, Fe, Cu, W, Pb, and U targets, in the particle energy range 0.01-5000 GeV.

There is a disadvantage of existing GEANT4 classes for hadron-nuclear cross-sections: the energy-dependence of the cross-sections for $E > 100$ GeV is wrong. Existing implementations either have a large relativistic rise (LHEP) or are constant above 100 GeV (QGSP). To correct this, a new GG implementation for total and inelastic hadron cross-sections has been developed. It utilizes a simplified version of the Glauber model with Gribov improvements. According to the GG model the total σ_{tot}^{hA} and inelastic σ_{in}^{hA} cross-sections of a hadron on a nucleus with atomic weight A are:

$$\sigma_{tot}^{hA} = 2\pi R^2 \ln\left[1 + \frac{A\sigma_{tot}^{hN}}{2\pi R^2}\right],$$

$$\sigma_{in}^{hA} = \pi R^2 \ln\left[1 + \frac{A\sigma_{tot}^{hN}}{\pi R^2}\right].$$

Here σ_{tot}^{hN} is the particle data group parameterization [26] of total hadron-nucleon cross-section, and R is the root mean square of the Gaussian distribution of the nucleon density in the nucleus.

An additional implementation of cross-sections for protons and neutrons using Barashenkov's evaluations [24] has been initiated to account for the low-energy behavior below 1 GeV.

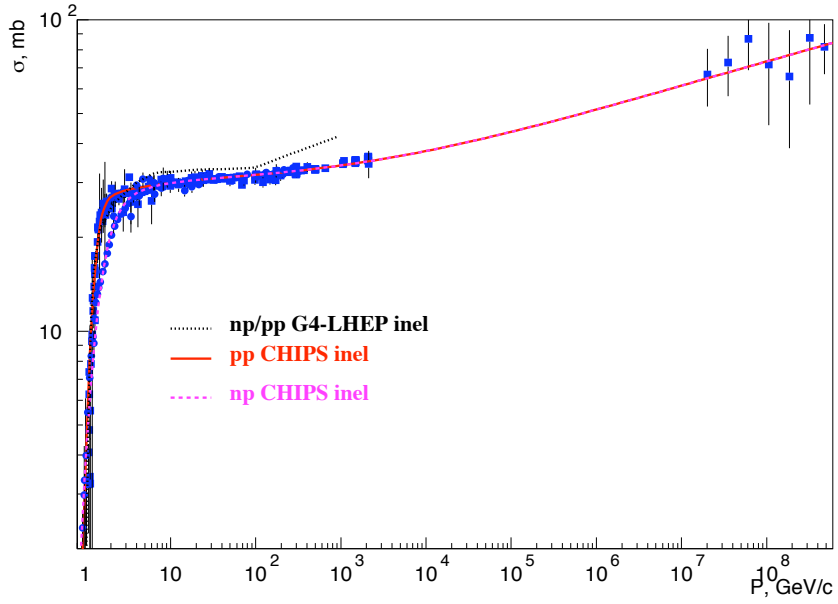

Figure 10: Inelastic cross-sections of protons (squares) and neutrons (circles) on Hydrogen from [26].

Figures 7-9 show comparisons between GEANT4 model predictions and experimental data [27]-[28], for the inelastic proton and neutron cross-sections on different targets (Fe, Cu, Pb) commonly used in hadronic calorimeters. For energies above 1 GeV the agreement with experimental data [27]-[28] is at the level of $10-20\%$. The expected small relativistic rise for energies above 100 GeV is reproduced in the "GG" model. The low energy region is reasonably well described by Barashenkov's evaluations [24]. The combination of these models could provide a good simulation of hadron-nuclear cross-sections for pions and nucleons in the wide energy range 0.01-5000 GeV.

For light nuclei, where parameterization should be more accurate, a new approximation can be used, which fits with high accuracy the $n-H$ and $p-H$ data (Fig.10 - solid line).

Figures 11 and 12 show the comparison of different GEANT4 models with experimental data for Helium-4 and Beryllium, respectively. For comparison, an approximation of the ENDF-VI [29] is shown by a dashed line. It is close to data and to the new approximation (solid line), while it covers only cross-sections below 20 MeV.

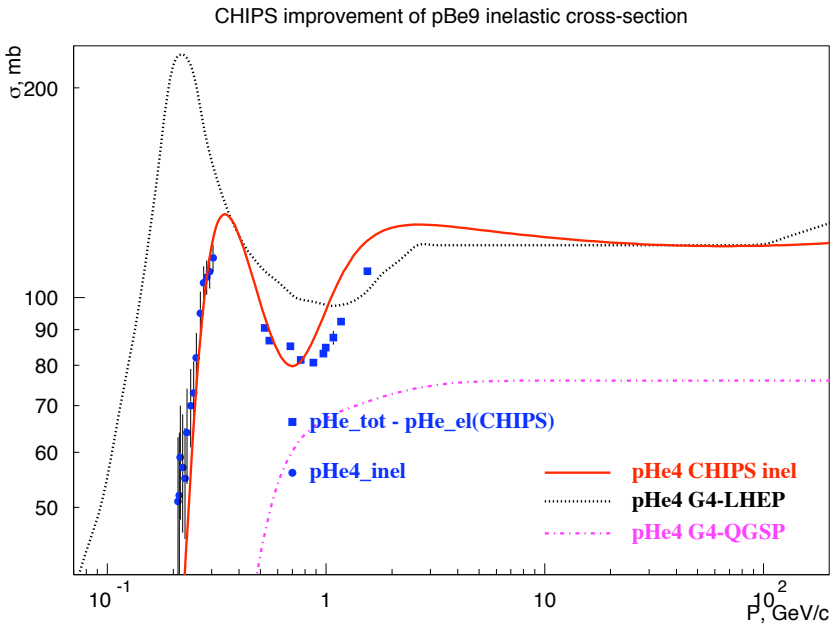

Figure 11: Inelastic cross-sections of protons on Helium, squares are calculated as a difference of measured total cross-sections and calculated CHIPS elastic cross-sections.

8 Elastic scattering

Elastic scattering of hadrons directly affects the development of hadronic showers in matter. For hadronic calorimeters with scintillators, the energy transfer from low-energy neutrons to recoiling nuclei is dominated by neutron elastic scattering on protons of the scintillator. Given its relevance for hadronic showers, we decided to review the GEANT4 models for hadron elastic processes.

In GEANT4 , two models were initially available for elastic scattering: G4LElastic derived from the GHEISHA package, and G4NeutronHPElastic developed only for transportation of low-energy neutrons, applicable for kinetic energies below 20 MeV. There are G4pp and G4np models in GEANT4 which are based on SAID fit [30] in the energy range 20 - 1000 MeV. In the Physics Lists relevant to the shower shape problem the GHEISHA-type G4LElastic model was used. It was shown that this model is very approximate, especially for the description of scattering on Hydrogen nuclei.

A new theory-based model, G4ElasticHadrNucleusHE, has been developed over some time. This model uses the Glauber approach [31], with corrections for inelastic screening [32], and total cross-section [33]. Tuning of this Glauber-type model have been performed using different data for protons and pions [34]. Results for scattering of π^+ on protons are shown in Fig.13, which demonstrates that the new model agrees with the data, satisfactorily reproducing the main forward diffractive maxi-

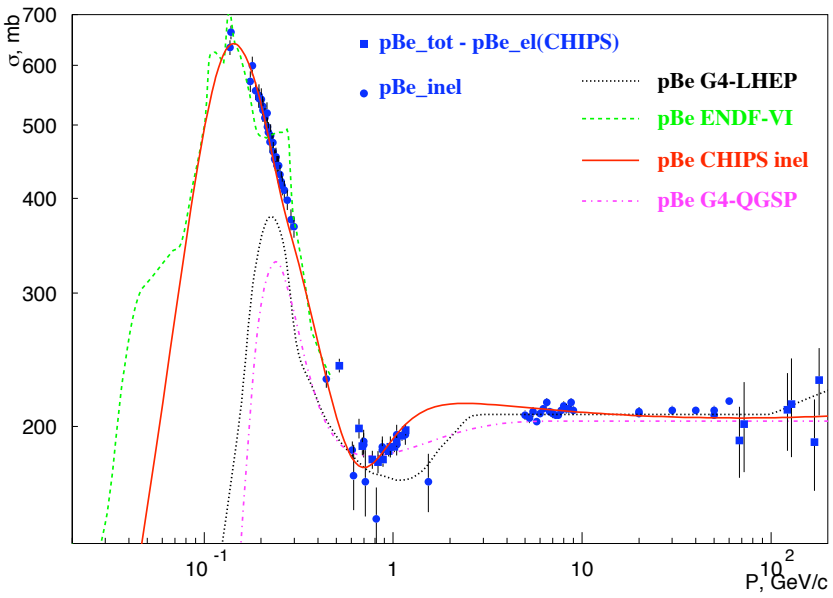

Figure 12: Inelastic cross-sections of protons on Beryllium, squares corresponde to the difference between measured total cross-sections and calculated CHIPS elastic cross-sections.

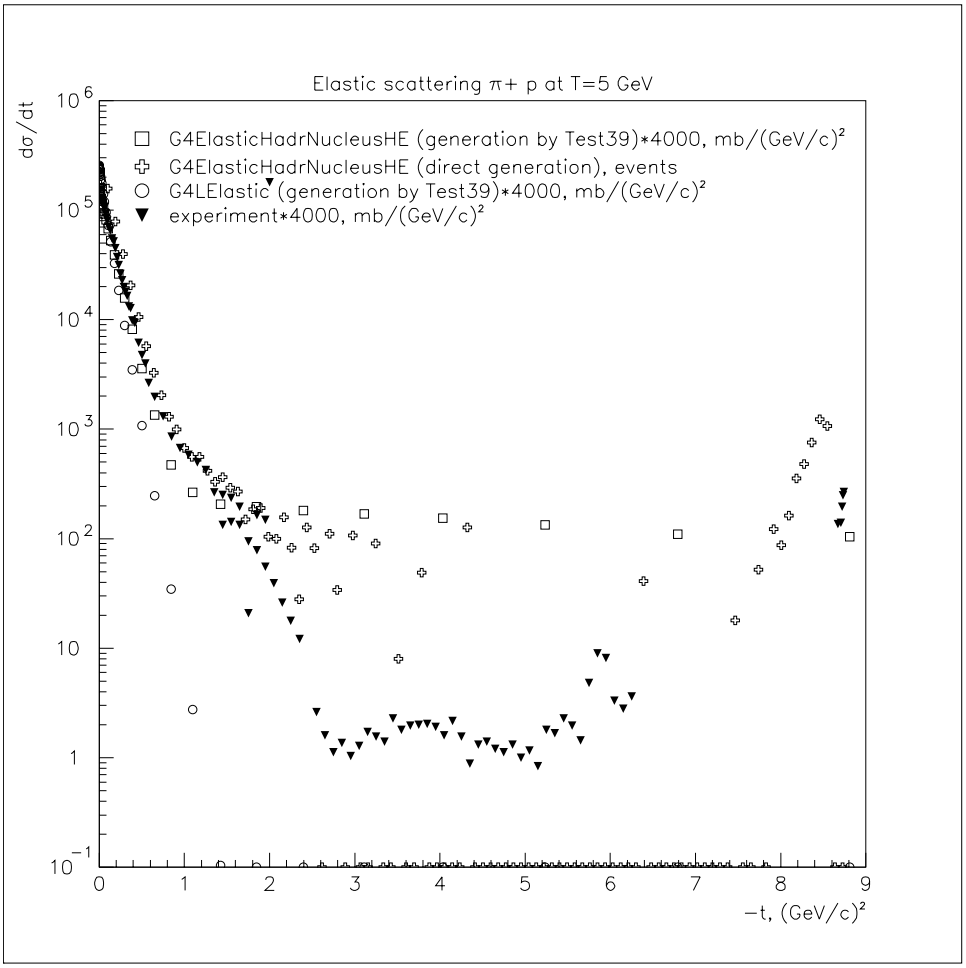

Figure 13: Differential elastic cross-sections of π^+ scattering on Hydrogen target. Experimental data (triangles) are from [34], results of simulation with GHEISHA-type mode (open circles) and Glauber-type model (open squares).

mum, whereas scattering at large angle is less well reproduced. The GHEISHA-type model is a long way from the data.

An advantage of the Glauber approach is the possibility to create a model applicable to all types of hadrons. Unfortunately, this approach is valid only for initial energies above 1 GeV. Recently, the area of application of the model has been formally extended down to 400 MeV (*i.e.* above the resonance region) but it still does not cover the whole energy range for hadrons, which is important for hadronic showers.

An alternative approach was developed in the CHIPS sub-package of GEANT4 . A phenomenological model was tuned using a huge amount of experimental data. The parameterization of the CHIPS elastic cross-sections for protons and neutrons (a new G4QElastic process) is based on the analysis of about 600 papers with about 3000 data-sets for differential proton-nuclear scattering on ^1H, ^2H, ^3He, ^4He, ^6Li, ^7Li, Be,

C, Al, Cu, Sn, and Pb targets. As a result, a precise analytic parameterization of the total and elastic cross-sections were made. The main improvement is connected with the correct calculation of the recoiling nucleus. The CHIPS simulation of the $n-H$ scattering is important for calorimeters that use scintillators as active material. This parameterization has been included in GEANT4 within the G4HadronElastic model in the QGSP Physics List starting with release 8.1. This partial CHIPS implementation is less important for liquid Argon calorimeters, where Hydrogen is not present.

The typical distributions of neutron-Hydrogen scattering are shown in Fig.14. The dotted lines show the GEANT4 SAID (G4Lnp class) angular distributions, which are normalized by the LHEP elastic cross-sections. One can see that at low energies (205 MeV/c) the normalization is wrong, while the angular distribution is satisfactory. A possible explanation for the too large LHEP cross-section can be given by the G4LElastic angular distribution (dashed lines). One can see that the charge exchange part of the distributions (large t) is exaggerated in LHEP. On the other hand, at 0.5 GeV/c the charge exchange part does not exist at all, while in data it is definitely present. One can see that at this momentum the GEANT4 (data-driven) SAID model fits the data as well as the new G4QElastic process (solid line). At 1.4 GeV/c G4LElastic (LHEP Physics List) still significantly overestimates the small angle scattering and underestimates the large angle scattering, while at high energies it does not produce the recoiling nucleus, and that is why it is not shown for 23.4 GeV/c. At high energies, the GEANT4 SAID model (which is not yet used in any Physics List) does not fit the data too. The new G4QElastic process describes well the $n-H$ elastic data at all energies.

For light nuclei it is difficult to separate elastic and quasi-elastic spectra, because they have similar slopes, but at low energies it is possible to resolve the ground state mass of the scattered nucleus and disentangle the elastic scattering from the quasi-elastic scattering. At high energies this is instead impossible. In Fig.15 one can see that at low energies (26 and 276 MeV/c) the LHEP $p-C$ elastic cross-section is underestimated and at all energies the differential cross-section has an unreasonable minimum at $t=-0.006\ GeV^2$. In addition, even for the light nucleus one can see that the LHEP elastic scattering includes both elastic and quasi-elastic scattering, while the inelastic cascade models simulate the quasi-elastic scattering too. This additional part is seen at 1.46 GeV/c, and the measurements at 175 GeV/c, which include quasi-elastic scattering, are well fitted by the G4HadronElastic model, which confirms the inclusion of the quasi-elastic scattering. The new G4QElastic process (solid lines) does not include quasi-elastic scattering and fits the $p-C$ elastic data at all energies satisfactorily.

The double counting of the quasi-elastic scattering is better seen for heavy nuclei. Fig.16 shows proton-lead elastic scattering. Comparison of angular distributions at 492 MeV and 175 GeV/c confirms the conclusion, which was already made for the proton-carbon scattering, while by unknown reason the large angle $p-Pb$ scattering at 1.46 GeV/c is not present at all. Instead, the simulated angular distribution

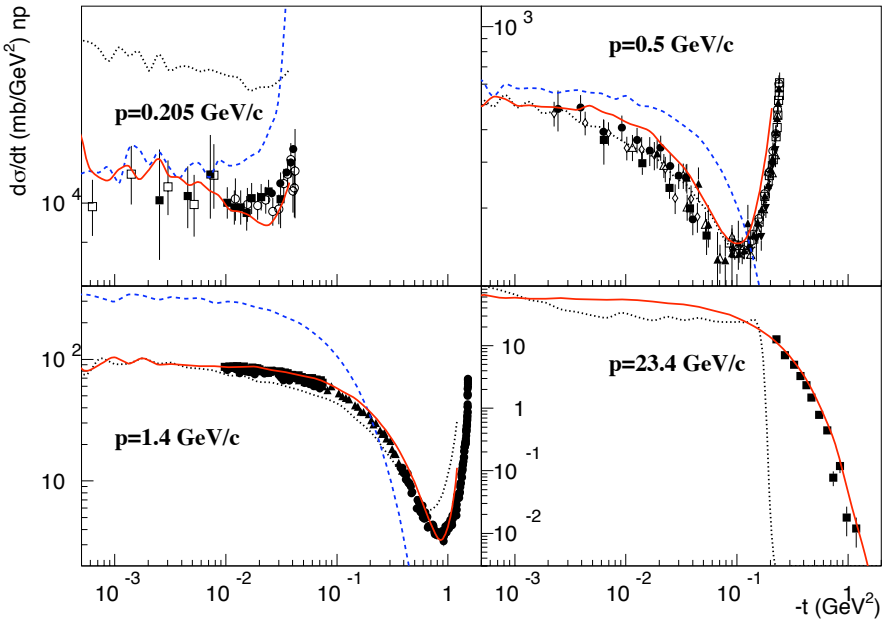

Figure 14: CHIPS improvement of $n-p$ elastic scattering. Solid line G4QElastic, dashed lines are G4LElastic, dotted lines are G4Lnp (GEANT4 SAID) with GEANT4 LHEP elastic cross-sections normalization.

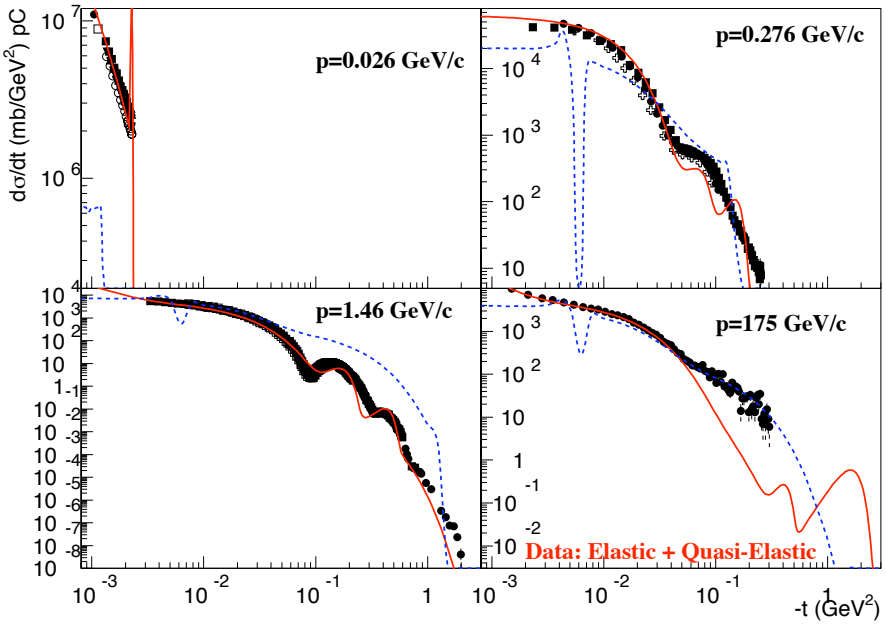

Figure 15: CHIPS improvement of $p - C$ elastic scattering. Solid line G4QElastic, dashed lines are G4HadronElastic (modified G4LElastic, used in QGSP Physics List).

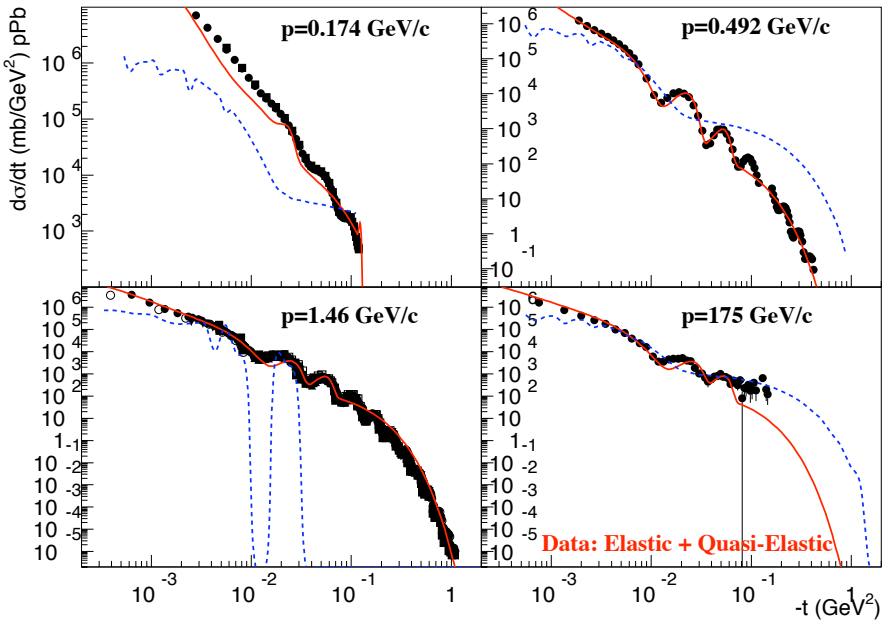

Figure 16: CHIPS improvement of $p - Pb$ elastic scattering. Solid line G4QElastic, dashed lines are G4HadronElastic.

becomes very irregular. On the other hand, the new G4QElastic process fits the data satisfactorily. In CHIPS approximation only the forward diffraction maximum and the two secondary maxima have been fitted separately, and the rest of the diffraction distribution was fitted by an exponential function.

The neutron-nuclear elastic cross-sections have the same CHIPS approximation as for proton-nuclear (without interference with the electromagnetic scattering at low angles). For neutrons, special efforts have been applied to improve the simulation at very low energies, in order to offer to the users an alternative to the slow HP package. The low energy neutron-nuclear cross-sections have been parametrized for all isotopes. The improved version of the G4QElastic process is applicable for any target nucleus. In GEANT4 release 8.2 it is included in the QGSC Physics Lists.

Due to the availability of different models applicable for different energy ranges and different target nuclei, a new process G4UHadronElasticProcess and a new model G4HadronElastic were created for GEANT4 release 8.1. These new classes provide the best combinations of cross-sections and GEANT4 models for reference Physics Lists, combining the CHIPS-model for Hydrogen, the Glauber-type model for high energies, and the modified GHEISHA-type model, which now conserves energy and produces the recoiling nucleus. As a backup solution for mesons at low energies, isotropic S-wave scattering is used in absence of an advanced model, while at low energies mesons

create P-wave resonances, and the angular distribution is anisotropic. The low energy meson-nuclear elastic scattering needs further improvement.

9 Neutrons

Neutrons can influence the shower shape by propagating further than charged particles through material and hence depositing energy in the "tails" of the hadronic shower. Within GEANT4 neutrons can be handled in a number of ways depending upon energy and model choice. If the interaction is elastic then there are three different models:

- G4LElastic - this is part of the GHEISHA/LHEP parametrized models within GEANT4 and specifically below a certain energy threshold actually produces no scattering (reduces CPU time).

- G4HadronElastic - this combines CHIPS/s-wave depending upon energy and target. See Sec.8 for further description.

- G4NeutronHPElastic - this is part of the neutronHP package which handles neutrons using a data-base approach sampling both the cross-section and the final states. This is currently applicable for neutron energies below 20 MeV, although the data-base is planned to be extended up to 3 GeV for certain isotopes.

For inelastic interactions the same model choice is available as for protons, although below 20 MeV the high precision neutronHP model can be deployed. The inelastic component includes gamma production, capture, secondary nucleon emission and fission.

Neutrons can be produced from a primary high energy interaction, lower energy cascades or secondary interactions at intermediate energy. The pre-compound and evaporation models are particular prevalent sources. From thin target low energy studies it is clear that the Binary cascade under-produces neutrons, whilst the Bertini-type cascade over-produces. Conversely, the Binary cascade produces a harder neutron spectrum than Bertini-type cascade and is much closer to the measured double-differential spectra.

In order to further understand the production, interaction and transportation of neutrons a comparison was made with the TARC experiment [35]. This is a moderate energy thick target validation, whereby 2.5 GeV/c protons impinged on a large lead block approximately cylindrical with a diameter of 3.3 m [36].

From the inclusion of cascade and neutronHP models within the shower shape simulation it was seen that some improvement was achieved, but only in the tails of the distribution.

10 Diffraction

Diffraction is expected to play a role in the longitudinal hadronic shower development, given the fact that diffractive particles are almost always leading ones. On nuclei the coherent sum of the diffraction amplitudes of different nucleons can increase the diffractive contribution. To test quickly how the simulation of diffraction can impact the longitudinal hadronic shower profile, we did the following simple exercise: we enhanced the diffractive component of the Quark Gluon String model in the QGSP Physics List by an arbitrary scaling factor, and then studied the effect on a simplified calorimeter set-up. For a 300 GeV π^- beam on a simplified Cu-LAr calorimeter, where normal QGSP Physics List is producing showers significantly shorter than LHEP Physics List, with a diffractive scaling factor of 3 the modified QGSP produces hadronic showers with the same longitudinal profile as LHEP. See table 4 for the results for some values of the diffractive scaling factor.

The factor 3 should not be taken too seriously, but this exercise shows clearly the need to investigate whether the current implementation of the diffraction in GEANT4 is correct, both in terms of its cross-sections and its final-state kinematics.

In parallel, the tuning of the diffraction part of the interaction should be improved on the basis of the existing experimental data. There are plenty of data on diffraction for p-p and p-$\overline{p}$ collisions, at different energies (ISR, SpS, Tevatron), but unfortunately there is very little available for nucleon-nucleus diffraction, and practically nothing for pion-nucleus diffraction.

We plan to validate the forward physics of GEANT4 , mainly diffraction but also including elastic and quasi-elastic, using the SPY/NA56 measurement of charged particle production from 450 GeV/c protons on beryllium [37].

Another interesting direction of research, closely related to diffraction, is the quasi-elastic process. This is essentially an elastic interaction of the incoming hadron with a single nucleon, with a final state typically consisting of the initial hadron only slightly scattered and a free nucleon, with the remnant nucleus in the ground state. Currently QGS does not include the quasi-elastic process; however, the inelastic cross-sections used by QGS do include the contribution of quasi-elastic. This means that the effective *production* — or *deep-inelastic* — cross-section is overestimated by the contribution of the neglected quasi-elastic process, which implies showers that develop too quickly and are therefore too short. At the time of writing, we are doing some preliminary and qualitative assessment of this effect — the first results are promising. Our plan is to include a proper model of the quasi-elastic process in GEANT4 and validate it with thin-target data.

11 Pions and Kaons models below 10 GeV

From the tables 1, 2, and 3 it can be seen that the fraction of produced π^0, with respect to the total number of pions, is around 38% [1] higher than the expected value, 1/3. Indeed, there is only one Physics List that shows this expected, lower value: QGSP_BERT.

Given the fact that the electromagnetic fraction of a hadronic shower is strongly correlated with the shower profile, and this fraction is dominated by the process $\pi^0 \to \gamma\gamma$, we have investigated what is producing the observed π^0 fractions in GEANT4 . Table 5 reports, for the case of a 100 GeV π^- beam on a Cu-LAr sampling calorimeter (a simplified version of ATLAS HEC), comparisons between the following Physics Lists:

- LHEP : the parametrized Physics List, which comprises of two models: LEP (Low Energy Parametrized) below 55 GeV, and HEP (High Energy Parametrized) above 25 GeV (in the interval 25-55 GeV the two models are both active, and at each interaction one of the two is randomly selected according to a probability that is descreasing linearly from 1 to 0 for LEP, and increasing linearly from 0 to 1 for HEP).

- QGSP_BERT : the default "Quark Gluon String + Precompound + Bertini-type cascade" Physics List, where the parametrized model LEP is used down to 9.5 GeV, and Bertini-type cascade is used below 9.9 GeV.

- 4.5-4.9 : a modified version of QGSP_BERT, where, for pions and kaons, the parametrized model LEP is extended down to 4.5 GeV, and Bertini-type cascade is used only below 4.9 GeV.

- 3.5-3.9 : a modified version of QGSP_BERT, where, for pions and kaons, the parametrized model LEP is extended down to 3.5 GeV, and Bertini-type cascade is used only below 3.9 GeV.

- 2.5-2.9 : a modified version of QGSP_BERT, where, for pions and kaons, the parametrized model LEP is extended down to 2.5 GeV, and Bertini-type cascade is used only below 2.9 GeV.

- piKlep : a modified version of QGSP_BERT, where, the parametrized model LEP is extended down to 0 for pions and kaons without using Bertini-type cascade at all (notice that this modified Physics List differs from QGSP because for protons and neutrons Bertini-type cascade is utilised).

From these comparisons, it follows that the LEP model is responsible for the unnaturally high fraction of π^0 produced in all Physics Lists, with the only exception

[1] This value would be even higher, around 1/2, if we use the default GEANT4 , *i.e.* without setting the environmental variable AlwaysKillLeadingHadron. See section 5 for more information.

of QGSP_BERT which uses the Bertini-type cascade instead of LEP for pions (and kaons) below 10 GeV. It is likely that the LEP model over-production of π^0 at low energies is an artifact to compensate for the HEP model under-production of π^0 at high energies. As the LEP and HEP models are used together, as in the LHEP Physics List, they manage somehow to produce reasonably good hadronic showers. This is not the case when the LEP model is used together with other high-energy models, namely Quark Gluon String or Fritiof, because it produces a too high electromagnetic fraction, which in turn implies that the showers are shorter and narrower than what they would be otherwise. Finally, the reason why QGSP_BERT seems to be better than all the other non-parametrized Physics Lists in describing hadronic showers is because it replaces the LEP model below 10 GeV with a better model (Bertini-type cascade).

In conclusion, it appears that to improve the hadronic shower description in GEANT4 we need to find a replacement for the LEP model, at least for pions below 10 GeV.

12 Trying out other models: INCL+ABLA, QGSC_EFLOW, and Fritiof

Recently, we have tried out another three independent models in GEANT4 .

One is the "INCL+ABLA" model [38], which offers a "cascade" alternative to Bertini-type or Binary, for primary particles of kinetic energy below about 1.6 GeV. A proper new C++ version of INCL+ABLA for GEANT4 is under development, so we have used for this study a temporary C++ wrapper around the original Fortran code. A new internal Physics List, named QGSP_INCL, allows the use of the INCL+ABLA model together with QGSP. Table 6 reports the comparisons of shower profile variables between some Physics Lists, for 100 GeV π^- on a Cu-LAr calorimeter. As can be seen, no significant changes in either the longitudinal or the lateral shower profiles are observed with QGSP_INCL.

Recently, the QGSC Physics List was updated with a better description of nuclear fragmentation in high energy nuclear reactions. The main idea of the QGSC (QGS + CHIPS: see section 12) Physics List is to absorb soft particles produced by the Quark Gluon String projectile fragmentation by the residual nucleus. The summed energy of the absorbed soft particles should be about $T(b) * \frac{dE}{dx}$, where $T(b)$ is the nuclear depth at the randomized value of the impact parameter b and $\frac{dE}{dx}$ is the energy depositon rate for high energy hadrons in nuclear matter. The QGSC Physics List uses $\frac{dE}{dx} = 1.0\frac{GeV}{fm}$ and suggests that each absorbed hadron is interacting independently with nuclear matter and creates its own "quasmon" excitation in nuclear matter with "multi-quasmon" fragmentation of the nucleus in final state. The QGSC_EFLOW Physics List uses $\frac{dE}{dx} = 1.5\frac{GeV}{fm}$, and combines all absorbed hadrons in an energy flow and creates only one quasmon. Comparison with data [18] shows that the nuclear

fragmentation part is described better by QGSC_EFLOW, providing more hadrons in the nuclear fragmentation region. Thus one can expect that the QGSC_EFLOW Physics List provides wider shower shapes. This is confirmed by the simulation of 100 GeV π^- on a Cu-LAr calorimeter, as shown in table 6.

The other model tested was the Fritiof model (FTF, see section 12) [39], the diffractive string excitation model which offers an alternative of Quark Gluon String model at high-energy. Indeed, we have tried out two variants of it, all embedded in the FTFP Physics List, which uses Precompound for the de-excitation and evaporation part:

- FTFP : the default Fritiof as present in the distributed Physics List FTFP;
- FTFP': as the previous one, with some updated parameters according to the current experimental and theoretical understanding of diffraction (see section 6 for more information).

Table 7 reports the comparisons of shower profile variables between these two variants of the Fritiof model (with LHEP and QGSP for reference) for 300 GeV π^- on a Cu-LAr calorimeter.

Some work is currently undergoing to further improve and extend the Fritiof model.

13 Conclusions and outlook

In this note we have presented some of the studies aimed at improving the simulation of hadronic shower shapes in GEANT4 .

The strategy that has been followed relies on two complementary approaches: macroscopic, based on simplified calorimeter set-ups, which allow the assessment of the effect of different Physics Lists on the development of hadronic showers; microscopic, based on thin target experimental data, to validate, tune, and improve single physics processes.

Several calorimeter observables have been compared between different Physics Lists, using negative pion beams at different energies (30, 100, and 300 GeV) impinging on a simplified Copper-Liquid Argon sampling calorimeter without instrumental effects.

Some simple benchmarks results have been presented for high-energy models, where single- or double-differential distributions — in which the typical variables can be the rapidity, momentum, transverse momentum and longitudinal scaled momentum (*i.e.* Feynman x_F) — are compared against experimental data.

Snapshots of the studies of some of the most important physics aspects for the development of hadronic showers have been reported, covering the following items: hadronic cross-sections; elastic scattering; neutron production and transportation; diffraction; and meson production.

From the work that has been carried out so far in order to understand and improve the simulation of hadronic showers, our main conclusions and prospects for future work are the following:

- Intranuclear cascade models produce longer and wider hadronic shower shapes; they also improve the energy resolution (*i.e.* reduce σ_E/E) and lower the ratio e/π.

- An improved description of hadronic elastic scattering is now in place, and this produces hadronic showers slightly wider than before, approaching the data.

- Refinement of existing high-energy models and investigations of alternative ones could provide new insights on hadronic shower shapes.

- Diffraction can have a significant impact on longitudinal hadronic shower shapes. We need to start a thorough validation on data of the diffraction modelling in GEANT4 .

- In GEANT4 (perhaps with the only exception of LHEP), the quasi-elastic hadronic process is not simulated, although its cross-section is included in the inelastic cross-section, and this can affect significantly the longitudinal development of hadronic showers. Therefore, we need to include the modelling of quasi-elastic interactions in GEANT4 , and then validate it on thin-target data.

- We have realized that the parametrized treatment of pions and kaons below 10 GeV, which is used in almost all Physics Lists (with the only exception of QGSP_BERT) is overestimating the π^0 production, causing the showers to be a little shorter; therefore, we have to replace this model with a better one.

- Cross-sections can have a dramatic influence on shower shapes, therefore the validation and revision of all GEANT4 cross-sections, based on published data and recent theoretical development, must continue.

- Finally, for users who need immediately a good simulation of shower shapes, we suggest either the Physics List LHEP, or, if more precise physics is needed in general (e.g. for energy response and resolution), QGSP_BERT. Experiments (ATLAS and CMS, in particular) are currently validating this Physics List against their test-beam data.

Acknowledgment

We would like to thank Alfredo Ferrari, Michel Maire, Paola Sala, and Dennis Wright for useful discussions.

References

[1] R. Wigmans,
"Calorimetry: energy measurement in Particle Physics."
Oxford Science Publications (2000).

[2] Web page of "Physics Validation for LHC Simulations":
http://lcgapp.cern.ch/project/simu/validation

[3] S. Agostinelli *et al.*, GEANT4 Collaboration,
"GEANT4 - a simulation toolkit."
Nuclear Instruments and Methods in Physics Research, A 506 (2003) 250.
J. Allison *et al.*,
"GEANT4 developments and applications."
IEEE Transactions on Nuclear Science 53 No. 1 (2006) 270-278.
See also the GEANT4 web page: http://cern.ch/geant4.

[4] F. Gianotti *et al.*,
"GEANT4 hadronic physics validation with LHC test-beam data: first conclusions."
CERN-LCGAPP-2004-10, see http://lcgapp.cern.ch/project/mgmt/doc.html.

[5] GEANT4 Physics Reference Manual,
http://cern.ch/geant4/UserDocumentation/UsersGuides/PhysicsReferenceManual/html/

[6] GEANT4 Physics Reference Manual, Chapter 29: Precompound Model
available at http://geant4.web.cern.ch/geant4/support/userdocuments.shtml.

[7] H. Fesefeld,
"Simulation of hadronic showers, physics and applications."
Technical Report PITHA 85-02, Aachen, Germany, Sept. 1985.

[8] R.A. Arndt, I. I. Strakovsky, and R.L. Workman,
"Nucleon-nucleon elastic scattering to 3 GeV."
Phys. Rev. **C 62**, 034005 (2000).

[9] N.S. Amelin *et al.*, Phys. Rev. Lett. **67**, 1523 (1991);
N.S. Amelin *et al.*, Nucl. Phys. **A544**, 463c (1992);
L.V. Bravina *et al.*, Nucl. Phys. **A566**, 461c (1994);
L.V. Bravina *et al.*, Phys. Lett. **B344**, 49 (1995).

[10] N.V. Stepanov, ITEP Preprint ITEP-55, Moscow (1988).

[11] M.P. Guthrie, R.G. Alsmiller and H.W. Bertini, Nucl. Instr. Meth. **66**, 29 (1968);
H.W. Bertini and P. Guthrie,

"Results from Medium-Energy Intranuclear-Cascade Calculation."
Nucl. Phys. **A169**, (1971).

[12] G. Folger, V.N. Ivanchenko and J.P. Wellisch, Eur. Phys. J. **A21**, 407 (2004).

[13] M.V. Kossov,
"Manual for the CHIPS event generator."
KEK internal report 2000-17, Feb. 2001 H/R;
P.V. Degtyarenko, M.V. Kossov and J.P. Wellisch, Eur. Phys. J. **A8** (2), 217 (2000),
P.V. Degtyarenko, M.V. Kossov and J.P. Wellisch, Eur. Phys. J. **A9** (2), 211 (2001), and
P.V. Degtyarenko, M.V. Kossov and J.P. Wellisch, Eur. Phys. J. **A9** (2), 221 (2001).

[14] M.V. Kossov and L.M. Voronina, ITEP Preprint 165-84, Moscow (1984).

[15] J. J. Whitmore *et al.*,
"Inclusive charged pion production in hadron nucleus interactions at 100-GeV/c and 320-GeV/c."
Z. Phys. C **62** (1994) 199.

[16] Experimental Nuclear Reaction Data Retrievals database,
http://www.nea.fr/html/dbdata/x4 .

[17] N. A. Nikiforov *et al.*,
"Backward Production of Pions and Kaons in the Interaction of 400-GeV Protons with Nuclei."
Phys. Rev. C **22** (1980) 700.

[18] N. M. Agababyan *et al.*, EHS-NA22 Collaboration,
"Rapidity and transverse momentum structure in π^+ and K^+ collisions with Al and Au nuclei at 250-GeV/c."
Z. Phys. C **50** (1991) 361.

[19] R. J. Apsimon *et al.*, Omega Photon Collaboration,
"Inclusive production of π^0 mesons in π-p, K-p and γ-p collisions at energies around 100-GeV."
Z. Phys. C **52** (1991) 397.

[20] V. V. Abramov *et al.*,
"Production of hadrons with large $P^\perp$ in nuclei at 70 GeV."
Yad. Fiz. **41** (1985) 357, Sov. J. Nucl. Phys. **41** (1985) 227.

[21] C. Alt *et al.* [NA49 Collaboration], arXiv:hep-ex/0606028.

[22] T. Abbott *et al.*, E-802 Collaboration,
"Measurement of particle production in proton induced reactions at 14.6-GeV/c."
Phys. Rev. D **45** (1992) 3906.

[23] V.S. Barashenkov,
"Pion-Nucleus Cross-sections."
Preprint P2-90-158, Dubna 1990.

[24] V.S. Barashenkov,
"Nucleon-Nucleus Cross-sections."
Preprint P2-89-770, Dubna 1989.

[25] H.J. Wellisch, D. Axen,
"Total reaction cross-sections in proton-nucleus scattering."
Physical Review **C54** (1996) 1329-1332.

[26] pdg.lbl.gov.

[27] http://wwwppds.ihep.su.

[28] http://www.nea.fr/html/dbdata/bara.html.

[29] http://t2.lanl.gov.

[30] Program by Richard Arndt, see http://gwdac.phys.gwu.edu/ .

[31] R.J. Glauber, in "High Energy Physics and Nuclear Structure", edited by S. Devons, Plenum Press, NY, 1970.

[32] E.A. Abers *et al.*, Nuovo Cimento, **42** (1966) 365; V.N. Gribov, Zh. Eksp. Theor. Fiz., **18** (1973) 271.

[33] R.A. Nam *et al.*, Sov. Jour. of Nucl. Phys., **26** (1977) 550-555.

[34] G.D. Alkhazov *et al.*, Phys. Rep., **C42** (1978) 89-144.

[35] A. Abanades *et al.*, TARC Collaboration,
Nuclear Instruments and Methods in Physics Research, A 478 (2002) 577.

[36] A. Howard,
"Validation of Neutrons in GEANT4 *Using TARC Data: production interaction and transportation."*
IEEE Nuclear Science Symposium 2006.

[37] G. Ambrosini *et al.*, NA56/SPY Collaboration,
"Measurement of charged particle production from 450 GeV/c protons on beryllium."
Eur. Phys. J.C 10 (1999) 605.

[38] A. Boudard *et al.*,
"Intranuclear cascade model for a comprehensive description of spallation reaction data."
Phys. Rev. C66 (2002) 044615.

[39] B. Andersson, G. Gustafson, and B. Nielsson-Almquist,
"A model for low-pT hadronic reactions with generalizations to hadron-nucleus and nucleus-nucleus collisions."
Nucl. Phys. 281 (1987) 289.

Observable	LHEP	QGSP	QGSC	QGSP_BIC	QGSP_BERT	QGSP_BERT_HP
E_{vis}	1113 ± 2 MeV	1183	1160	1225	1277	1292
σ_E/E	13.6%	12.3%	13.8%	11.0%	9.5%	9.6%
e/π	1.30	1.22	1.24	1.18	1.13	1.12
f_{L1}	67.8 ± 0.5 %	66.3%	67.3%	65.3%	62.1%	61.6%
f_{L2}	26.3 ± 0.3 %	26.9%	26.3%	27.5%	29.5%	29.4%
f_{L3}	5.1 ± 0.1 %	5.8%	5.6%	5.9%	7.1%	7.4%
f_{L4}	0.8 ± 0.04 %	1.0%	0.9%	1.2%	1.4%	1.5%
f_{R1}	72.8 ± 0.3 %	76.1%	76.2%	72.7%	67.5%	66.7%
f_{R2}	23.7 ± 0.1 %	21.1%	21.0%	22.6%	25.8%	25.6%
f_{R3}	3.6 ± 0.04 %	2.8%	2.8%	4.7%	6.7%	7.7%
$\#EM$	25,931 ± 120	29,720	28,377	35,182	37,470	38,034
$\#\pi$	48 ± 0.1	39	39	41	37	37
π^0/π	38%	38%	38%	37%	32%	32%
$\#p$	140 ± 0.7	129	147	121	151	144
$\#n$	244 ± 1.1	247	272	445	807	647
L_n	136 ± 0.2 mm	185	127	330	361	887
exit_kin	1006 ± 15 MeV	816	955	906	789	779
exit_fn	23 ± 0.5 %	17%	19%	20%	22%	25%
exit_#n	23 ± 0.2	16	25	60	131	95
e_E_{vis}	61.9%	66.5%	64.9%	67.8%	66.7%	67.2%
e_f_{L1}	70.1%	69.8%	70.0%	68.7%	66.4%	65.7%
e_f_{L2}	24.9%	24.5%	24.5%	25.3%	26.8%	26.8%
e_f_{L3}	4.4%	4.9%	4.8%	4.9%	5.8%	6.3%
e_f_{L4}	0.6%	0.8%	0.7%	1.0%	1.1%	1.2%
e_f_{R1}	78.1%	81.4%	81.4%	77.3%	73.6%	72.5%
e_f_{R2}	19.7%	16.8%	16.8%	18.8%	20.4%	20.3%
e_f_{R3}	2.3%	1.8%	1.8%	4.0%	6.0%	7.3%
p_E_{vis}	16.9%	14.7%	16.4%	14.4%	17.2%	16.9%
p_f_{L1}	63.0%	57.8%	61.8%	54.9%	50.4%	50.1%
p_f_{L2}	29.3%	32.8%	29.8%	34.2%	36.8%	36.8%
p_f_{L3}	6.6%	7.9%	7.1%	9.0%	10.7%	10.9%
p_f_{L4}	1.1%	1.5%	1.3%	1.9%	2.1%	2.3%
p_f_{R1}	54.8%	58.0%	60.7%	55.1%	51.8%	51.2%
p_f_{R2}	36.1%	34.6%	32.5%	35.9%	39.5%	39.6%
p_f_{R3}	9.1%	7.4%	6.8%	9.0%	8.7%	9.2%
π_E_{vis}	13.6%	11.1%	10.9%	11.1%	12.4%	12.3%
π_f_{L1}	65.8%	62.2%	63.3%	62.3%	58.4%	58.1%
π_f_{L2}	27.5%	29.7%	28.9%	29.5%	32.1%	31.8%
π_f_{L3}	5.8%	6.9%	6.7%	6.8%	8.0%	8.4%
π_f_{L4}	0.9%	1.2%	1.2%	1.4%	1.5%	1.7%
π_f_{R1}	75.4%	75.3%	75.1%	74.3%	64.4%	64.1%
π_f_{R2}	23.0%	23.3%	23.3%	24.1%	31.4%	31.3%
π_f_{R3}	1.6%	1.4%	1.5%	1.6%	4.2%	4.5%
n_E_{vis}	7.1%	7.0%	7.2%	6.1%	3.0%	2.9%
n_f_{L1}	63.2%	59.4%	61.7%	58.0%	49.9%	51.0%
n_f_{L2}	29.2%	32.0%	30.1%	32.2%	37.0%	36.5%
n_f_{L3}	6.3%	7.4%	7.2%	8.1%	10.7%	10.2%
n_f_{L4}	1.2%	1.3%	1.0%	1.7%	2.3%	2.3%
n_f_{R1}	64.9%	66.4%	67.1%	61.4%	36.8%	36.2%
n_f_{R2}	29.6%	28.5%	27.8%	30.0%	43.0%	42.5%
n_f_{R3}	5.5%	5.1%	5.1%	8.6%	20.2%	21.3%
k_E_{vis}	0.2%	0.4%	0.4%	0.4%	0.3%	0.3%
μ_E_{vis}	0.3%	0.3%	0.3%	0.2%	0.2%	0.2%

Table 1: Comparisons between GEANT4 Physics Lists, for a 30 GeV π^- beam.

Observable	LHEP	QGSP	QGSC	QGSP_BIC	QGSP_BERT	QGSP_BERT_HP
E_{vis}	3884 ± 5 MeV	4064	4027	4192	4334	4376
σ_E/E	9.1%	8.0%	8.7%	7.0%	6.0%	6.0%
e/π	1.24	1.18	1.20	1.15	1.11	1.10
f_{L1}	52.6 ± 0.3 %	57.5%	58.1%	55.7%	54.1%	54.0%
f_{L2}	34.5 ± 0.2 %	32.1%	31.4%	32.6%	33.1%	33.4%
f_{L3}	10.3 ± 0.1 %	8.6%	8.5%	9.5%	10.2%	10.1%
f_{L4}	2.6 ± 0.1 %	1.8%	2.0%	2.2%	2.5%	2.6%
f_{R1}	76.1 ± 0.2 %	79.2%	79.6%	76.5%	72.2%	71.2%
f_{R2}	20.8 ± 0.1%	18.4%	18.0%	19.5%	22.2%	22.2%
f_{R3}	3.1 ± 0.02%	2.5%	2.4%	4.0%	5.7%	6.6%
$\#EM$	97,865 ± 337	110,884	108,989	127,757	134,262	135,276
$\#\pi$	134 ± 0.3	112	110	115	101	101
π^0/π	37%	38%	38%	38%	32%	32%
$\#p$	417 ± 2	373	399	350	431	412
$\#n$	722 ± 3	712	748	1287	2311	1851
L_n	140 ± 0.1 mm	189	128	339	368	920
exit_kin	3155 ± 85 MeV	2546	2624	2882	2449	2463
exit_fn	17 ± 0.4 %	13%	14%	16%	20%	23%
exit_#n	61 ± 0.3	43	75	163	365	253
e_E_{vis}	66.8%	72.1%	71.6%	73.6%	72.7%	72.7%
e_f_{L1}	55.6%	61.5%	61.8%	59.6%	58.9%	58.5%
e_f_{L2}	33.0%	29.9%	29.4%	30.6%	30.7%	31.0%
e_f_{L3}	9.1%	7.2%	7.2%	8.0%	8.4%	8.4%
e_f_{L4}	2.2%	1.4%	1.6%	1.8%	2.0%	2.0%
e_f_{R1}	81.8%	84.9%	85.2%	81.7%	78.7%	77.5%
e_f_{R2}	16.4%	13.7%	13.5%	15.2%	16.6%	16.7%
e_f_{R3}	1.8%	1.4%	1.4%	3.1%	4.7%	5.8%
p_E_{vis}	14.4%	12.5%	13.2%	12.0%	14.3%	14.5%
p_f_{L1}	44.5%	45.8%	47.8%	42.4%	39.1%	39.6%
p_f_{L2}	38.6%	38.6%	37.2%	39.3%	40.6%	40.9%
p_f_{L3}	13.5%	12.7%	12.0%	14.5%	15.9%	15.2%
p_f_{L4}	3.5%	3.0%	3.0%	3.8%	4.4%	4.3%
p_f_{R1}	55.6%	56.6%	59.1%	54.2%	51.8%	51.4%
p_f_{R2}	35.4%	35.8%	33.6%	36.9%	39.4%	39.4%
p_f_{R3}	9.0%	7.6%	7.3%	8.9%	8.7%	9.2%
π_E_{vis}	10.9%	8.8%	8.5%	8.7%	9.8%	9.8%
π_f_{L1}	47.2%	49.3%	49.7%	48.3%	45.3%	45.7%
π_f_{L2}	37.4%	36.7%	36.2%	36.8%	38.0%	38.2%
π_f_{L3}	12.3%	11.3%	11.4%	12.1%	13.2%	12.8%
π_f_{L4}	3.2%	2.6%	2.7%	2.9%	3.4%	3.4%
π_f_{R1}	74.3%	74.3%	74.4%	73.5%	63.3%	63.0%
π_f_{R2}	23.9%	24.1%	23.9%	24.8%	32.3%	32.4%
π_f_{R3}	1.7%	1.6%	1.6%	1.7%	4.5%	4.6%
n_E_{vis}	7.3%	6.0%	6.0%	5.0%	2.5%	2.4%
n_f_{L1}	49.9%	47.3%	49.4%	45.2%	40.0%	40.2%
n_f_{L2}	35.8%	37.8%	36.0%	38.0%	39.8%	39.8%
n_f_{L3}	11.4%	12.0%	11.8%	13.6%	15.8%	15.8%
n_f_{L4}	2.9%	2.9%	2.8%	3.2%	4.4%	4.3%
n_f_{R1}	67.6%	65.8%	67.1%	60.4%	37.0%	37.8%
n_f_{R2}	27.5%	29.0%	27.7%	30.9%	42.7%	41.7%
n_f_{R3}	5.0%	5.3%	5.2%	8.7%	20.2%	20.5%
k_E_{vis}	0.3%	0.3%	0.3%	0.3%	0.3%	0.3%
μ_E_{vis}	0.2%	0.2%	0.2%	0.2%	0.2%	0.2%

Table 2: Comparisons between GEANT4 Physics Lists, for a 100 GeV π^- beam.

Observable	LHEP	QGSP	QGSC	QGSP_BIC	QGSP_BERT	QGSP_BERT_HP
E_{vis}	11829 ± 13 MeV	12445	12343	12787	13131	13244
σ_E/E	7.0%	6.1%	6.6%	5.4%	4.5%	4.6%
e/π	1.22	1.16	1.17	1.13	1.10	1.09
f_{L1}	48.4 ± 0.3 %	50.2%	51.4%	50.5%	48.7%	47.9%
f_{L2}	35.9 ± 0.2 %	35.5%	34.6%	34.5%	35.5%	36.0%
f_{L3}	12.5 ± 0.1 %	11.4%	11.1%	11.8%	12.4%	12.3%
f_{L4}	3.3 ± 0.05%	2.9%	2.9%	3.2%	3.5%	3.7%
f_{R1}	78.3 ± 0.2 %	81.9%	82.3%	79.5%	75.6%	75.1%
f_{R2}	18.8 ± 0.1%	16.1%	15.7%	17.1%	19.5%	19.3%
f_{R3}	2.8 ± 0.01%	2.1%	2.0%	3.4%	4.9%	5.6%
$\#EM$	314,251 ± 888	361,455	356,569	404,997	420,312	423,865
$\#\pi$	362 ± 1	285	275	289	260	257
π^0/π	38%	39%	39%	38%	32%	32%
$\#p$	1152 ± 4	961	1011	883	1102	1043
$\#n$	2002 ± 7	1844	1903	3276	5945	4704
L_n	141 ± 0.1 mm	191	129	345	372	946
exit_kin	11192 ± 222 MeV	7999	8109	8810	8363	8086
exit_fn	12 ± 0.4 %	10%	11%	14%	16%	19%
exit_#n	164 ± 1	104	186	403	921	611
e_E_{vis}	70.5%	76.7%	76.4%	77.8%	76.7%	76.9%
e_f_{L1}	52.0%	54.4%	55.2%	54.5%	53.4%	52.6%
e_f_{L2}	34.4%	33.8%	33.0%	32.9%	33.6%	34.3%
e_f_{L3}	10.9%	9.6%	9.5%	10.1%	10.3%	10.2%
e_f_{L4}	2.7%	2.3%	2.3%	2.5%	2.7%	2.9%
e_f_{R1}	84.0%	87.2%	87.4%	84.5%	81.9%	81.2%
e_f_{R2}	14.4%	11.7%	11.5%	13.0%	14.2%	14.1%
e_f_{R3}	1.6%	1.2%	1.1%	2.5%	3.9%	4.7%
p_E_{vis}	13.1%	10.5%	11.1%	10.2%	12.3%	12.2%
p_f_{L1}	38.2%	35.3%	38.8%	34.5%	31.0%	30.4%
p_f_{L2}	40.0%	41.7%	39.9%	40.6%	42.6%	42.4%
p_f_{L3}	16.9%	17.8%	16.3%	18.8%	20.1%	20.5%
p_f_{L4}	4.8%	5.2%	4.9%	6.1%	6.4%	6.7%
p_f_{R1}	56.2%	56.6%	59.2%	54.4%	51.9%	51.7%
p_f_{R2}	34.9%	35.7%	33.3%	36.6%	39.4%	39.1%
p_f_{R3}	9.0%	7.6%	7.5%	9.0%	8.7%	9.2%
π_E_{vis}	9.5%	7.2%	7.1%	7.2%	8.3%	8.2%
π_f_{L1}	40.1%	38.0%	39.6%	38.7%	36.0%	35.3%
π_f_{L2}	39.4%	40.7%	39.9%	39.8%	41.0%	41.4%
π_f_{L3}	15.9%	16.5%	15.9%	16.5%	17.6%	17.7%
π_f_{L4}	4.5%	4.7%	4.6%	5.0%	5.4%	5.6%
π_f_{R1}	74.2%	74.2%	74.2%	73.1%	63.0%	62.7%
π_f_{R2}	23.9%	24.3%	24.2%	25.2%	32.4%	32.6%
π_f_{R3}	1.8%	1.6%	1.6%	1.7%	4.5%	4.6%
n_E_{vis}	6.4%	5.0%	4.9%	4.3%	2.2%	2.2%
n_f_{L1}	42.6%	36.9%	39.2%	37.0%	32.0%	31.8%
n_f_{L2}	38.3%	41.0%	39.6%	40.4%	41.8%	41.1%
n_f_{L3}	15.0%	17.1%	16.3%	17.3%	19.8%	19.8%
n_f_{L4}	4.2%	5.0%	4.9%	5.3%	6.4%	7.2%
n_f_{R1}	67.9%	65.8%	68.0%	60.7%	38.2%	40.3%
n_f_{R2}	26.9%	29.0%	27.5%	30.6%	42.2%	39.8%
n_f_{R3}	5.2%	5.2%	4.5%	8.7%	19.6%	19.9%
k_E_{vis}	0.3%	0.3%	0.3%	0.3%	0.3%	0.3%
μ_E_{vis}	0.2%	0.2%	0.2%	0.2%	0.2%	0.1%

Table 3: Comparisons between GEANT4 Physics Lists, for a 300 GeV π^- beam.

Observable	LHEP	QGSP	QGSPx2	QGSPx3	QGSPx4	QGSPx10
E_{vis}	11829 ± 13 MeV	12445	12445	12445	12453	12401
f_{L1}	48.4 ± 0.3 %	50.2%	49.6%	47.9%	46.9%	38.9%
f_{L2}	35.9 ± 0.2 %	35.5%	35.1%	35.9%	35.7%	37.0%
f_{L3}	12.5 ± 0.1 %	11.4%	12.1%	12.7%	13.2%	17.3%
f_{L4}	3.3 ± 0.05%	2.9%	3.2%	3.5%	4.1%	6.7%
f_{R1}	78.3 ± 0.2 %	81.9%	81.8%	81.9%	82.1%	83.2%
f_{R2}	18.8 ± 0.1%	16.1%	16.2%	16.1%	15.9%	14.9%
f_{R3}	2.8 ± 0.01%	2.1%	2.0%	2.0%	2.0%	1.9%

Table 4: Comparisons between different values of the diffractive scaling parameter in QGSP Physics List, for a 300 GeV π^- beam on a Cu-LAr calorimeter.

Observable	LHEP	QGSP_BERT	piKlep	2.5-2.9	3.5-3.9	4.5-4.9
E_{vis}	3884 ± 5 MeV	4334	4157	4260	4276	4298
f_{L1}	52.6 ± 0.3 %	54.1%	55.8%	55.3%	54.7%	54.7%
f_{L2}	34.5 ± 0.2 %	33.1%	33.0%	33.2%	32.6%	33.2%
f_{L3}	10.3 ± 0.1 %	10.2%	9.1%	9.3%	10.3%	9.9%
f_{L4}	2.6 ± 0.1 %	2.5%	2.1%	2.2%	2.4%	2.3%
f_{R1}	76.1 ± 0.2 %	72.2%	76.4%	74.1%	73.5%	73.0%
f_{R2}	20.8 ± 0.1%	22.2%	19.3%	20.9%	21.3%	21.6%
f_{R3}	3.1 ± 0.02%	5.7%	4.4%	5.0%	5.2%	5.4%
$\#\pi$	134 ± 0.3	101	110	107	105	103
π^0/π	37%	32%	36%	33%	33%	33%

Table 5: Comparisons between GEANT4 Physics Lists, for a 100 GeV π^- beam on a Cu-LAr calorimeter. See the text for the meaning of the last four columns, which represents variations of the QGSP_BERT Physics List.

Observable	LHEP	QGSP	QGSP_INCL	QGSC	QGSC_EFLOW
E_{vis}	3884.4 ± 5 MeV	4063.5	3810.2	4026.9	4046.1
σ_E/E	9.1%	8.0%	11.8%	8.7%	8.3%
e/π	1.24	1.18	1.26	1.20	1.19
f_{L1}	52.6 ± 0.3 %	57.5%	58.7%	58.1%	57.6%
f_{L2}	34.5 ± 0.2 %	32.1%	31.3%	31.4%	31.9%
f_{L3}	10.3 ± 0.1 %	8.6%	8.1%	8.5%	8.6%
f_{L4}	2.6 ± 0.1 %	1.8%	1.8%	2.0%	1.9%
f_{R1}	76.1 ± 0.2 %	79.2%	77.8%	79.6%	79.1%
f_{R2}	20.8 ± 0.1 %	18.4%	17.3%	18.0%	18.3%
f_{R3}	3.1 ± 0.02%	2.5%	4.9%	2.4%	2.6%

Table 6: Comparisons between QGSP_INCL and QGSC_FLOW Physics Lists with LHEP and QGSP, for 100 GeV π^- beam on a Cu-LAr calorimeter.

Observable	LHEP	QGSP	FTFP	FTFP-retuned
E_{vis}	11829 ± 13 MeV	12445	12623	12599
σ_E/E	7.0%	6.1%	6.3%	6.6%
f_{L1}	48.4 ± 0.3 %	50.2%	50.9%	50.9%
f_{L2}	35.9 ± 0.2 %	35.5%	35.1%	35.1%
f_{L3}	12.5 ± 0.1 %	11.4%	11.3%	11.1%
f_{L4}	3.3 ± 0.05%	2.9%	2.8%	2.9%
f_{R1}	78.3 ± 0.2 %	81.9%	81.0%	81.0%
f_{R2}	18.8 ± 0.1%	16.1%	16.8%	16.8%
f_{R3}	2.8 ± 0.01%	2.1%	2.2%	2.2%

Table 7: Comparisons between two different variants of the FTFP Physics List (see the text) and LHEP and QGSP, for a 300 GeV π^- beam on a Cu-LAr calorimeter.